Surface-Anchored Polymer Chains: Their Role in Adhesion and Friction

Liliane Léger[1,2], Elie Raphaël[1,3] and Hubert Hervet[1,4]

[1] Laboratoire de Physique de la Matière Condensée, URA 792 du CNRS, Collège de France, 11 Place Marcelin-Berthelot, 75231 Paris Cedex 05, France
[2] *e-mail: lleger@ext.jussieu.fr*
[3] *e-mail: elie@ext.jussieu.fr*
[4] *e-mail: hervet@ext.jussieu.fr*

Polymer surfaces and interfaces have many technological applications. In the present article we review some recent experiments conducted on model systems with the aim of understanding the role played by surface-anchored polymer layers in adhesion and friction. We also discuss some of the related theoretical models. The key parameter for both situations is the degree of interdigitation between the surface layer and the bulk polymer system (an elastomer in the case of adhesion, a molten polymer in the case of friction). We analyze how this degree of interdigitation governs the optimum enhancement in the adhesion energy between the solid wall and an elastomer, and how it is at the origin of the various wall slip regimes observed experimentally.

Keywords. Polymers, Interfaces, Grafted chains, Adsorbed chains, Polymer brushes, Adhesion, Friction, Chains pull out, Slip at the wall

Advances in Polymer Science, Vol.138

1 Introduction

In recent years, a large amount of experimental and theoretical work has been devoted to surface-anchored polymer chains [1–3]. Particular attention has been paid to polymer chains tethered by one end to a solid surface. At high enough coverage, the polymer chains stretch away from the surface forming a polymer "brush" [4]. As shown by Alexander and de Gennes in their pioneering work on polymer brushes [5, 6], the behavior of such end-grafted chains is qualitatively different from that of free chains. For a polymer brush in a good solvent, for instance, the layer thickness L is expected to vary *linearly* with the index of polymerization of the chains, N, while the radius R of a free chain in a dilute solution varies as $R \propto N^{3/5}$. The Alexander-de Gennes model was followed more recently by self-consistent field (SCF) calculations [7–13] and by computer simulations [14–16]. Several review articles on the subject are now available [17–20].

It is commonly admitted that polymer brushes should be quite efficient in many technological applications including in particular the steric stabilization of colloidal suspensions [21–23]. Because of these potential practical applications, strong experimental efforts have been devoted to characterize the structure and the properties of polymer brushes [1, 24]. These efforts, however, have long been slowed down by the difficulty to reach sufficiently high grafting densities in good solvent. Indeed, as soon as the first grafted chains begin to overlap, they repel each other. This, in turn, creates a repulsive barrier for the other chains and the grafting reaction almost stops. The resulting layer then consists of adjacent "mushrooms" [4]. A way to get around this difficulty was proposed by Auroy and co-workers [25–27]. It consists in performing the grafting reaction in a relatively concentrated solution where a rather large number of chains are located in the vicinity of the surface and are susceptible of being grafted. The particular system used by Auroy et al. was α-ω-hydroxyl terminated polydimethylsiloxane (PDMS) chains end-grafted on previously modified porous silica beads (by esterification of most of the silanol sites of the surface by pentanol molecules). An important result of the work of Auroy et al., apart from the demonstration of the possibility of forming chemically end-grafted brushes with high grafting densities, is the fact that the grafting density can be adjusted via the volume fraction of free polymer in the reaction bath. A derived way of modifying the silica surface, adaptable to plane large areas, has been developed recently and will be detailed in Sect. 2.1.

Let us mention at this point that a number of studies have used block copolymers in order to test the Alexander-de Gennes description of polymer brushes. For example, surface force measurements have provided some global character-

istics of the layers formed by block copolymers where one block adsorbs strongly on the substrate while the other block adsorbs negligibly [28, 29]. Diblock copolymer monolayers on the surface of a selective solvent have been studied by surface pressure measurements and by neutron reflectivity [30–32]. Block copolymers phases have also been investigated [33]. In these phases, the density of chains tethered to the interface is fixed by the equilibrium conditions of the self-assembly process and can not be chosen independently of the polymerization index, contrary to what can be done with chemically end grafted chains.

When a strongly attractive surface is exposed to a polymer melt, a certain amount of polymer becomes permanently bound to the surface. This occurs, for instance, when an untreated silica surface is exposed to a melt of PDMS [34]. If the polymer layer is then exposed to a good solvent, the layer swells. The resulting layer is made of loops, with a large polydispersity of loop sizes, reflecting the statistics of the chains in the melt state. The structure of such irreversibly adsorbed layers when swollen by a good solvent has been worked out by Guiselin [35]. Irreversibly adsorbed layers have been named "pseudo-brushes", because they are somewhat analogous to highly polydisperse brushes of loops. A comparison of brushes and pseuso-brushes in terms of adhesive and friction properties was seen as an interesting problem, and is one of the objectives of this paper.

The present paper is organized as follows. In Sect. 2 we present an experimental system for which both chemically end-grafted layers with high grafting densities and irreversibly adsorbed surface anchored layers can be formed (Sect. 2.1). We then discuss how the internal structure of these two kinds of surface layers can be analyzed and compared to the different available models (Sect. 2.2). In Sect. 3, we review what is expected for the interdigitation between such surface-anchored layers and a polymer melt, and compare these expectations with neutrons reflectivity results. In Sects. 4 and 5, we analyze the experimental data and the different models which allow to understand under which conditions such surface anchored layers can be used to promote adhesion or to reduce friction.

2
Formation and Characterization of the Surface Layers

2.1
Formation of the Surface Layers

There are several ways of forming surface layers of polymer chains, and various solid/polymer systems have been used. The silica/PDMS system is quite convenient since both end-grafted layers with high grafting densities (i.e., brushes) and irreversibly adsorbed layers (i.e., pseudo-brushes) can be formed with controlled molecular characteristics (polymerization index of the tethered chains and surface density), allowing a detailed investigation of the structure and properties of these two different classes of surface anchored polymer layers.

The irreversibly adsorbed layers are the easier to obtain. PDMS forms hydrogen bonds between the silanol sites of the silica surface and the oxygen atoms of the backbone of the chains, and thus spontaneously adsorbs on a clean silica surface. This adsorption is quasi permanent [36], and can be rendered permanent by using di-hydroxyl terminated PDMS chains. Incubation of the surface with a polymer solution (polymer volume fraction ϕ_0) at 120 °C during 12 h, leads to either condensation of the OH extremities of the chains on silanol sites of the silica, or to double hydrogen bond formation and the surface chains appear immobilized [37]. Then the layer can be washed by a good solvent in order to rinse away all the unattached chains, and dried. The monomers of the surface attached chains then collapse, and form a layer with a thickness directly related to the surface density of the anchored chains. The characteristics of these dry layers can be investigated through X-ray reflectivity techniques [38]. The electronic density inside the layer appears to be comparable to that of the polymer melt, and the dry thickness of the layer, h_0, is governed by both the polymerization index of the surface attached chains, N, and the volume fraction in the solution used for the incubation, ϕ_0. A collection of typical results for h_0, obtained through X-ray reflectivity or ellipsometry, on layers made with chains having polymerization indices in the range 10^2 to 10^4, is reported in Fig. 1, either for incubation from a melt (triangles, ϕ_0=1) or from a solution (squares and discs,

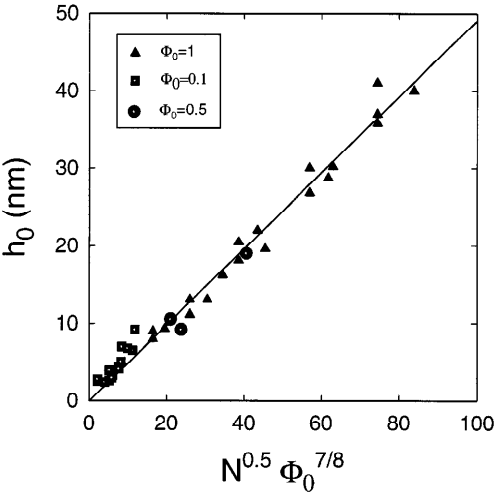

Fig. 1. Dry thickness h_0 of various PDMS layers irreversibly adsorbed on the silica surface of a silicon wafer, as a function of the scaling variable $N^{1/2}\phi_0^{7/8}$. N is the polymerisation index of the surface anchored chains and ϕ_0 is the polymer volume fraction in the incubation bath. The triangles correspond to ϕ_0=1, i.e., to the maximum surface density of anchored chains for the particular molecular weight. The range of molecular weights used is 29.6 kg mol^{-1}≤M_w≤740 kg mol^{-1}, with M_w=mN, where m is the molar mass of the monomer, m=0.074 kg mol^{-1} for PDMS

$10^{-1} \leq \phi_0 < 1$). A clear scaling law is observed, with the scaling variable $N^{1/2}\ \phi_0^{7/8}$. The origin of this scaling law can be easily understood: when the reaction cell is filled, all the polymer chains located in a layer from the surface with a thickness comparable to the radius of the chains in the incubation solution can rapidly find the surface and bind, keeping the local concentration equal to the bulk polymer concentration. Further adsorption of additional chains implies an increase of the local monomer concentration close to the surface (the chains already attached being not able to go away) and corresponds to a repulsive osmotic pressure. Thus the adsorption process stops when all the chains initially located in the surface layer with a thickness comparable to the radius of the chains in the incubation bath have adsorbed. Note that this is quite different from what occurs in the case of r*eversible* adsorption where the chains can permanently exchange between the surface layer and the bulk solution. In the case of reversible adsorption, the adsorbed layer can reach its thermodynamic equilibrium structure, which has been analyzed in terms of a self similar concentration profile [39–41]. For the irreversibly adsorbed layer, the structure is governed by the incubation bath and keeps track of the history of the layer formation. Such irreversibly adsorbed layers can however be put into an environment different from the incubation bath, keeping the surface density of anchored chains constant. Since the radius R of a chain in a semidilute solution scales like $R \cong a N^{1/2} \phi_0^{7/8}$ under good solvent conditions [42], one can easily count the number of monomers per unit surface area inside the surface layer and obtain for the adimensional surface chain density, σ, the following form: $\sigma \cong N^{-1/2} \phi_0^{7/8}$ (the number of chains per unit area, ν, is equal to σ / a^2, where a is the size of a monomer). Each chain containing N monomers of size a, the thickness of the dry surface layer is

$$h_0 \cong a N^{1/2}\ \phi_0^{7/8} \tag{1}$$

The data reported in Fig. 1 follow this scaling law, and give for the typical size of the monomer, $a \approx 0.5$ nm, a quite reasonable value for PDMS.

In order to form high density end-grafted layers with the same silica/PDMS system, one has to chemically modify the silica surface in order to suppress the monomers adsorption, while still keeping the possibility of end-grafting. An elegant way to do so has been developed by Folkers et al. [43]. It consists in first forming on the silica surface a self assembled monolayer of a short PDMS oligomer made of four monomeric units, and terminated by a chlorine at one extremity and either a Si-H or a Si-vinyl at the other one. The corresponding synthesis and monolayer formation are described in details somewhere else [43]. On such a self assembled monolayer, PDMS hardly adsorbs: under incubation conditions similar to those used to form the surface adsorbed layers, only a layer with a typical thickness of 1 nm remains fixed on the surface (probably adsorbed chains in the holes of the monolayer), to be compared with the 20–50 nm deposited in the case of bare silica with the same polymer and same conditions. On the functionalized extremities of the molecules in the monolayer, mono vinyl or Si-H end terminated long PDMS chains can be grafted by a hydrosililation reaction,

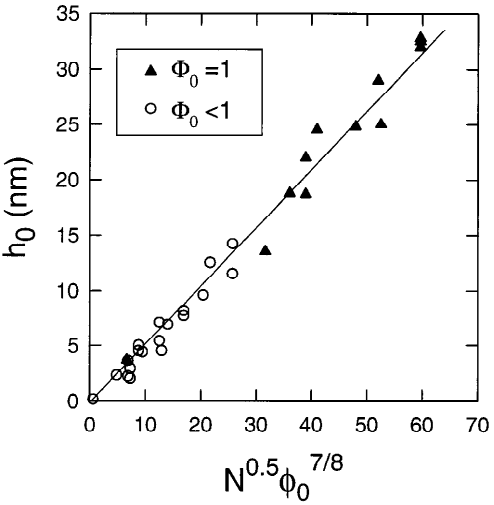

Fig. 2. Dry thickness h_0 f various PDMS layers end grafted on the modified silica surface of a silicon wafer, as a function of the scaling variable $N^{1/2}\phi_0{}^{7/8}$, with N the polymerisation index of the grafted chains and ϕ_0 he polymer volume fraction in the reaction bath. The range of molecular weights used for the grafted chains is 5 kg mol^{-1}≤M_w≤263 kg mol^{-1}, M_w=mN, with m=0.074 kg mol^{-1}

in the presence of platinum as catalyst [38, 43]. Again, and for reasons quite similar to what has been said for the adsorbed layers, the surface density in the grafted layer is governed by both the volume fraction in the reaction bath and the polymerization index of the PDMS chains used. The value of the dry thickness of the layer, h_0, determined after rinsing with a good solvent and drying, is a measurement of the surface density of grafted chains. Typical results for h_0, for a variety of PDMS chains and several volume fractions in the reaction bath are reported in Fig. 2. The same scaling law (Eq. 1) as for the irreversibly adsorbed chains is observed, with, at the accuracy of the experiments, the same prefactor, a≈0.5 nm. This means that the dry thickness of the layers, h_0, is a good measurement of the surface density of the surface anchored chains, but does not tell any information on the internal structure of the two categories of layers, irreversibly adsorbed and end-grafted, which, as we will see below, are quite different.

2.2
Characterization of the Internal Structure of the Surface Layers

In order to investigate the internal organization of the surface-anchored chains, we now consider the concentration profile of the layers when swollen by a good solvent. Such concentration profiles have been investigated in details theoretically, since the Alexander-de Gennes model, and we can hope to be able to dis-

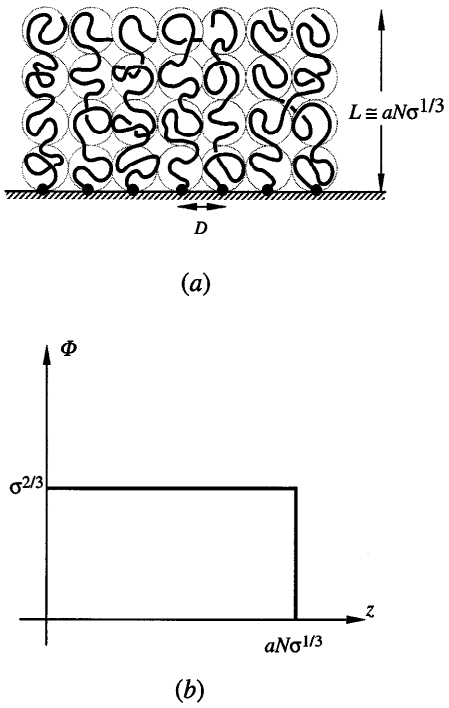

Fig. 3.a Schematic representation of a polymer brush. L is the layer thickness and D the average spacing between two grafting points. **b** The monomer density profile Φ vs distance from the grafting plane z according to the Alexander-de Gennes model. Figure adapted from [66]

criminate between different internal organizations and different models by comparing experiments and theoretical predictions.

Let us first briefly review the Alexander-de Gennes model [5, 6]. Specifically, we consider an ensemble of polymer chains, with degree of polymerization N, terminally grafted onto a flat surface and exposed to a solvent of low molecular weight. The number of terminally grafted chains per unit area is σa^{-2}, where a is the monomer size. The average distance between two grafting sites is given by $D=a\sigma^{-1/2}$. At low coverage, the different coils do not overlap (the so-called mushroom regime) and each chain occupies roughly a half-sphere with a radius comparable to the Flory radius of a free chain $R \cong aN^{3/5}$ (for simplicity reasons we assume the solvent to be athermal, i.e. $v \cong a^3$, where v is the excluded-volume parameter). When the grafting density, σ, becomes greater than the critical density $\sigma_0 \cong N^{-6/5}$ the different chains begin to overlap and form a brush of thickness L, as schematically presented in Fig. 3. The equilibrium structure of the brush results from the competition between the osmotic forces that tend to expand the layer and the restoring elastic forces. Accordingly, the free energy per chain can be written as $F=F_{os}+F_{el}$. In a Flory type approach, the elastic free energy is given

by $F_{el} \cong kTL^2/(a^2N)$ while the osmotic free energy is given by $F_{os} \cong kTa^3N^2/(LD^2)$. By minimizing F we obtain

$$L \cong a N \sigma^{1/3} \tag{2}$$

and $F \cong kTN\sigma^{3/2}$. Thus the brush thickness increases *linearly* with N. It is possible to develop a more refined scaling analysis of the overlap regime $\sigma > \sigma_0$ [5, 6]. A grafted chain is subdivided into blobs of size D, each containing g_D monomers. Within one blob, the chain behaves like a free excluded volume chain; this leads to the relation $D \cong a g_D^{3/5}$. Different blobs repel each other and the brush is essentially a closely packed system of blobs. The monomer volume fraction, Φ, is given by $\Phi \cong g_D(a/D)^3 \cong \sigma^{2/3}$. Since the volume per grafted chain is LD^2 the monomer volume fraction can be written as $\Phi \cong Na^3/LD^2$. Comparing the above two expressions for Φ we obtain the equilibrium brush height $L \cong aN\sigma^{1/3} \cong (\frac{N}{g_D})D$. This last result indicates that the chain can be viewed as a string of blobs almost fully stretched along the normal to the wall (see Fig. 3). The kT per blob ansatz leads to a free energy per chain $F \cong kTN\sigma^{5/6}$. Note that while the Flory analysis gives a correct estimate of the brush height, it overestimates the brush free energy.

The above Alexander-de Gennes model constrains the concentration profile to be steplike and all free ends to be at the same distance from the surface. This imposes strong restrictions on the allowed chains configurations. Some years ago, Hirz [7] and Cosgrove et al. [8] numerically solved the self-consistent field (SCF) equations describing the brush situation, but relaxing the above-mentioned restrictions. They found that in the case of a good solvent the concentration profile was essentially parabolic. This was rationalized analytically by Milner et al. [10, 11] and Zhulina et al. [12]. Much of the physics of the parabolic profile may be understood in terms of the following simple argument due to Pincus [44]. The mean-field free energy per unit area of the brush, H, may be written

$$\mathrm{H} = kT \int \frac{dz}{a^3} \left[\frac{1}{2}\phi^2(z) + \frac{1}{2Na^2} z^2 \Psi(z) - \mu \phi(z) \right] \tag{3}$$

where $\phi(z)$ and $\Psi(z)$ are respectively the monomer concentration and the free end concentration at a distance z from the surface. The first two terms in the integral, respectively, represent the excluded-volume energy and the polymer stretching energy; μ is a Lagrange multiplier to fix N monomers per chain. The problem is to determine $\Psi(x)$. A crude approximation may be obtained by guessing that far enough from the surface $\Psi(x) \cong \phi(x)/N$. Now setting $\delta H/\delta\phi(c) = 0$, we obtain a parabolic profile $\phi(x) \cong \left[\mu - \frac{1}{2}(x/Na)^2 \right]$ where $\mu \cong (3^{2/3}/2)(a/D)^{4/3}$ and the brush thickness $L \cong Na(3a^2/D^2)^{1/3}$ is consistent with the Alexander-de Gennes result (Eq. 2).

We now turn to pseudo-brushes. Five years ago, an elegant scaling approach has been proposed by Guiselin [35] to describe the irreversible adsorption from a polymer melt onto a plane surface, assuming that the time necessary to saturate all the surface sites was small compared to that of chain diffusion in the bulk. The conformation of the chains is thus not modified during the adsorption process and the distribution of loops and tails is related to the statistics of the chain folding in the melt. Guiselin considered the following sequence of events: (i) the plane solid surface is put in contact with a polymer melt and all the monomers touching the surface adsorb instantaneously and irreversibly; (ii) the surface is then washed with a pure solvent and only the initially adsorbed chains are retained onto the surface. The layer thus formed can be visualized as a succession of loops and tails. In the Guiselin's approach, each loop made of $2n$ monomers is considered as two pseudotails of n monomers. The number (per unit area) of pseudotails made of more than n monomers is given by [35]

$$S(n) \cong a^{-2} n^{-1/2} \qquad (1<n<N) \tag{4}$$

where, as for the brush, N is the degree of polymerization of the adsorbed chains and a the size of the monomer. When swollen by a good solvent, the pseudo-tails tend to stretch normal to the surface in order to decrease the excluded volume interactions. Let us assume that the n-th monomers of all pseudotails larger than n are located at the same distance z from the surface. We can then consider n as a function of z. At a distance z from the surface, the average distance between two pseudotails is given by $D(z) \cong \left[S(n(z))\right]^{-1/2}$. Using Eq. (4) we get $D(z) \cong a n^{1/4}(z)$ $(1<n<N)$. By analogy with the Alexander-de Gennes' model for monodisperse polymer brushes (see above) we expect that, locally, at a distance z from the surface, the layer can be visualized as a closely packed system of units of size $D(z)$. In order to determine the function $n(z)$, we consider the number $g(z)$ of monomers within a volume $[D(z)]^3$. The function $n(z)$ satisfies the differential equation $dn/g(z) = dz/D(z)$. At a scale smaller than D, the chain behaves like a free chain and g is related to D by the relation $g \cong (D/a)^{5/3}$ and, consequently, $n(z) \cong (z/a)^{5/6}$. The volume fraction of monomers is then given by

$$\Phi(z) \cong \left(D(z)/a\right)^{-4/3} \cong \left(a/z\right)^{-2/5} \tag{5}$$

and the total extension of the layer scales as

$$L \cong a N^{5/6} \tag{6}$$

The internal structure of a Guiselin's pseudo-brush is schematically presented in Fig. 4. Similar arguments in the case of an irreversibly adsorbed layer pre-

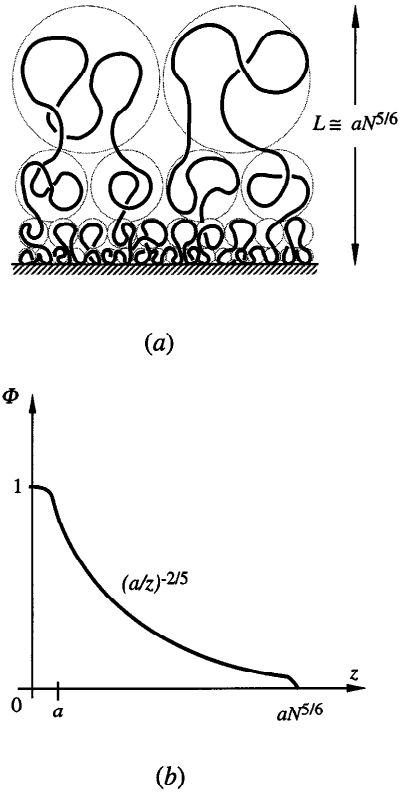

Fig.4.a Schematic of a pseudo-brush. *L* is the layer thickness. **b** The monomer density profile Φ vs distance from the grafting plane *z* according to Guiselin. Figure adapted from [66]

pared by adsorption from a semidilute solution with a volume fraction ϕ_0, lead to an extension of the layer that scales as $L \equiv aN^{5/6}\phi_0{}^{7/24}$ [35].

Systematic investigations of the concentration profile inside the two kinds of PDMS surface anchored layers have been performed through neutrons reflectivity techniques [45]. Octane was used as a good solvent and PDMS with a molecular weight of 92 kg mol^{-1}was either grafted or adsorbed on the surface of a silicon wafer, taking advantage of the contrast for neutrons between hydrogenated and deuterated species (either the solvent or the surface chains were deuterated). Fitting procedures of the reflectivity data have been developed in order to extract the concentration profile from the reflectivity curves, without assuming a priori the shape of the concentration profile, contrary to what is usually done [45]. The profile was divided into 10 or 20 slabs of equal thickness, and the index for neutrons of each slab was adjusted in order to obtain the best fit to the reflectivity curve. Despite the large number of adjustable parameters, this fitting pro-

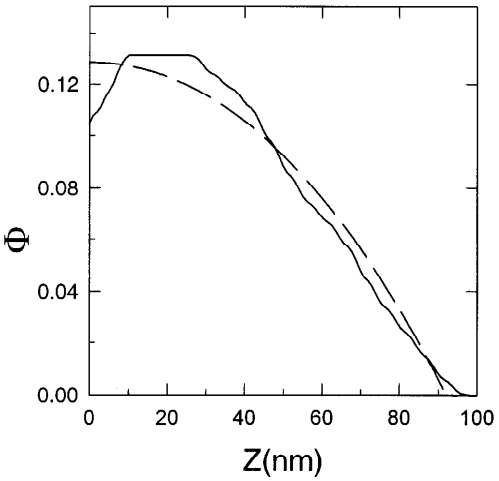

Fig. 5. Concentration profile inside a grafted PDMS layer swollen by a good solvent (octane). The molecular weight of the grafted chains is 92 kg mol^{-1} and the surface density in the layer is σ=0.011. The *full line* is the profile determined by neutrons reflectivity. The *dotted line* is the SCF result of Zhulina et al. [52] calculated for a surface density σ=0.011 and an excluded volume parameter v=0.8 a^3 (a is the size of the monomer, determined to be a≈0.5 nm by the slope of the scaling line in Fig. 2).

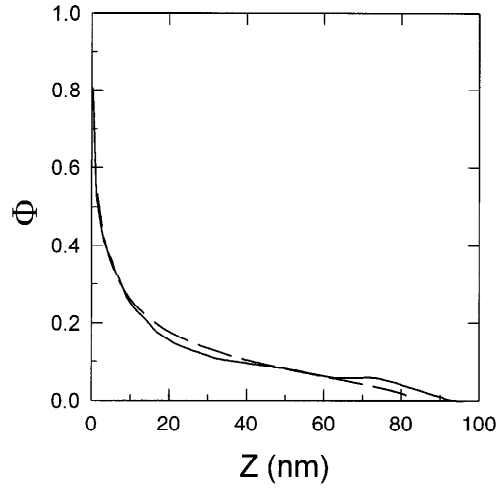

Fig. 6. Concentration profile inside an irreversibly adsorbed PDMS layer swollen by a good solvent (octane). The molecular weight of the adsorbed chains is 92 kg mol^{-1}. The surface density in the layer is σ=0.02. The *full line* is the profile determined by neutrons reflectivity. The *dotted line* corresponds to the theoretical profile calculated following the Guiselin's argument corrected to take into account the finite length of the surface chains [45]

cedure revealed to be quite efficient, provided one imposes a condition to favour smooth profiles and checks that the total surface excess of polymer, is equal to that measured independently by the dry thickness of the layer, h_0. In Figs. 5 and 6, typical concentration profiles for respectively a end-grafted layer (i.e. a brush) and an irreversibly adsorbed layer (i.e. a pseudo-brush) are reported.

In Fig. 5, the data points for the brush (full line) are compared to the calculated SCF parabolic profile of Milner et al. [10, 11] and Zhulina et al. [12]. In Fig. 6, the data points for the pseudo-brush (full line) are compared to the profile calculated by Guiselin [35]. Note that there are no adjustable parameters in the comparison between the theoretical predictions and the data points since the surface excess is imposed. The quite good agreement between the predicted and measured concentration profiles, and the very different shapes of the two curves for either the grafted or the irreversibly adsorbed layer are strong evidences of the fact that these layers have indeed quite different internal organization of the surface-anchored polymer chains. It is interesting to notice that, despite the good agreement between the experiments and the models for both kinds of layers, the two theoretical descriptions used are somewhat different: the parabolic profile is the result of an SCF analysis where the constrains on the allowed chains configurations imposed by the Alexander-de Gennes model are relaxed, while the Guiselin's description treats the layer at a degree of approximation comparable to the Alexander-de Gennes approach (the only difference being in the polydispersity of the pseudo-tails). While it clearly appears that the experimental concentration profile of the end-grafted layer cannot be described by the step profile of the scaling Alexander-de Gennes model (see Fig. 5), it seems that the Guiselin's model is sufficient to describe the experimental concentration profile of the irreversibly adsorbed layer (this might be due to the large polydispersity of loop sizes [11, 66]).

3
Interdigitation Between Surface-Anchored Chains and a Polymer Melt

In order to understand the role played by surface-anchored chains in adhesion and friction, it is essential to understand under which conditions a surface layer, when in contact with a melt, is penetrated by free chains. The question has been addressed theoretically mostly for polymer brushes, and more recently for Guiselin's pseudo-brushes. We want to review here some of these analysis, and compare the predictions of the models with the available experimental data.

3.1
Polymer Brushes in Polymeric Matrices

Most of the existing studies focus on brushes exposed to a low molecular weight solvent and less is known of the behavior of surface-tethered polymers in polymeric matrices [6, 46–56]. On the experimental side, nuclear reaction analysis [57, 58], neutron scattering [59–61], neutron reflectivity [62] and secondary-ion

mass spectrometry [63] have provided some information concerning the structure of grafted chains immersed in a polymer melt or a solution of mobile polymer chains. The first computer simulation of a brush immersed in a polymer melt was presented recently by Grest [64].

The case where the grafted chains are in contact with a melt of shorter, chemically identical chains was studied theoretically by de Gennes some years ago [6]. His approach has been further developed by Leibler [46], Raphaël et al. [51], and Aubouy et al. [54]. Consider a brush made of chains, with degree of polymerization N, terminally grafted onto a flat surface and exposed to a polymeric solvent made of chemically identical chains, with degree of polymerization $P<N$ (the effect of a small non-zero χ between the P and the N chains has been discussed by Aubouy and Raphaël [53]) The number of terminally grafted chains per unit area is σa^{-2}, where a is the monomer size. The average distance between two grafting sites is given by $D=a\sigma^{-1/2}$. At sufficiently low σ, the grafted chains do not overlap (the so-called mushroom regime) and the layer thickness L is given by $L\cong aN^{1/2}$ for $P>N^{1/2}$ and by $L\cong aN^{3/5}P^{-1/5}$ for $P<N^{1/2}$ (see regions {1} and {2} in Fig. 7). As σ increases, the different chains begin to overlap for $D\cong L$. This defines an overlap concentration: $\sigma_{ov}\cong N^{-1}$ for $P>N^{1/2}$ and $\sigma_{ov}\cong N^{-6/5}P^{2/5}$ for $P<N^{1/2}$. In a Flory-type approach the free energy per chain is then given by [6]

$$\frac{F}{kT}\cong\frac{L^2}{a^2N}+\frac{a^3}{P}\frac{N^2}{LD^2} \tag{7}$$

The first term in Eq. (7) represents the elastic contribution. The second term corresponds to the effect of the screened two-body interactions. From Eq. (7) one can easily construct the (P,σ) diagram represented in Fig. 7. In region {3}, two-body interactions are relevant and the brush thickness is obtained by minimizing Eq. (7): $(L=aNP^{-1/3}\sigma^{1/3}$. In region {4}, repulsive interactions are not sufficient to swell the brush and the conformation of a grafted chain remains Gaussian: $L\cong aN^{1/2}$. At higher σ, we reach region {5} where the P chains are almost completely expelled from the brush: the brush is "dry" [6]. The brush thickness L is then related to σ by the requirement $\Phi=aN\sigma/L\cong 1$ which leads to $L\cong aN\sigma$. The free energy per chain consists merely of an elastic term $F\cong kTL^2/a^2N\cong N\sigma^2$. The boundaries between regions {3} and {4} and between regions {3} and {5} are given by $\sigma\cong PN^{-3/2}$ and $\sigma\cong P^{-1/2}$, respectively.

According to the scaling theory [51, 54], region {3} has to be subdivided into two regions. In region {3a}, a grafted chain may be subdivided into spherical blobs of size D, each containing g_D monomers. Within one blob, the chain behaves like a free chain and can therefore be pictured as a self-avoiding walk of subunits called *melt blobs* [42, 51]. This leads to the relation $D\cong ag_D{}^{3/5}P^{-1/5}$. Different blobs repel each other and the brush is essentially a closely packed system of blobs. The volume fraction Φ of monomers belonging to grafted chains is given by $\Phi\cong g_D(a/D)^3\cong\sigma^{2/3}P^{1/3}$. Since on the other hand $\Phi=aN\sigma/L$, we obtain for the equilibrium brush thickness $L\cong aNP^{-1/3}\sigma^{1/3}$. This thickness can be rewritten as $L\cong(N/g_D)D$: the chain can be viewed as a string of blobs almost fully stretched

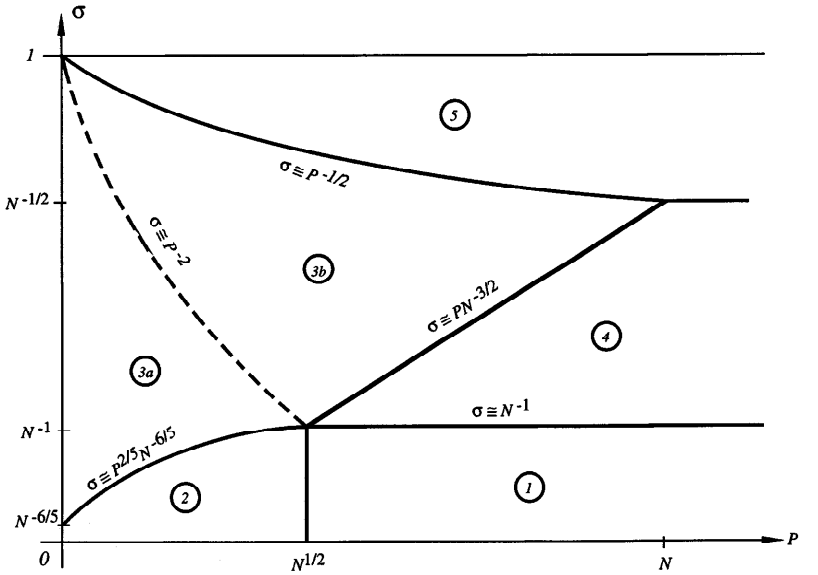

Fig. 7. Schematic (P, σ) diagram for a brush of polymerization index N exposed to a chemically identical melt of polymerization index P. At sufficiently low σ, the grafted chains do not overlap and the layer thickness L is given by $L \cong aN^{1/2}$ for $P > N^{1/2}$ (region {2}) and by $L \cong aN^{3/5}P^{-1/5}$ for $P < N^{1/2}$ (region {1}). As σ increases, the different chains begin to overlap for $\sigma \geq \sigma_{ov}$ where the overlap surface density is given by $\sigma_{ov} \cong N^{-1}$ for $P > N^{1/2}$ and by $\sigma_{ov} \cong N^{-6/5}P^{2/5}$ for $P < N^{1/2}$. In region {4}, two-body interactions are not sufficient to swell the brush and the conformation of a grafted chain remains Gaussian: $L \cong aN^{1/2}$. In region {3}, two-body interactions are relevant and the brush thickness is given by $L = aNP^{-1/3}\sigma^{1/3}$. At higher σ, region {5}, the P chains are almost completely expelled from the brush and the brush is "dry". The brush thickness L is then given by $L \cong aN\sigma$. The subdivision of region {3} into two regions (region {3a} and region {3b}) is discussed in the text. Figure adapted from [54]

along the normal to the wall. The kT per blob ansatz leads to a free energy per chain $F \cong kTNP^{-1/3}\sigma^{5/6}$. When the grafting density increases, the blob size D progressively decreases down to a point where it is of the order of the melt blob size $l_c \cong aP$. The crossover occurs for $D \cong aP$ that is for $\sigma \cong P^{-2}$ (this grafting density corresponds to the broken line in Fig. 7). Therefore, the blob picture developed above is only valid in region {3a} of the (P,σ) diagram. In region {3b}, each chain can be viewed as a string of non-overlapping spherical subunits, of size Λ larger than D, almost fully stretched along the normal to the wall (see Fig. 8). At a scale smaller than Λ, the chain behaves like an ideal chain of $g_\Lambda \cong (\Lambda/a)^2$ monomers. It is important to notice that in a plane parallel to the wall, subunits of different chains do overlap and therefore the brush as a whole cannot be described as a closely packed system of subunits (see Fig. 8). The subunit size is given by $\Lambda \cong aP^{1/3}\sigma^{-1/3}$ [54]. Since the different subunits of a grafted chain repel each other, the brush thickness is given by $L \cong \left(N/g_\Lambda\right)\Lambda \cong aNP^{-1/3}\sigma^{1/3}$, in agreement with the Flory result. The free energy per chain is given by $F/kT \cong N/g_\Lambda \cong NP^{-2/3}\sigma^{2/3}$.

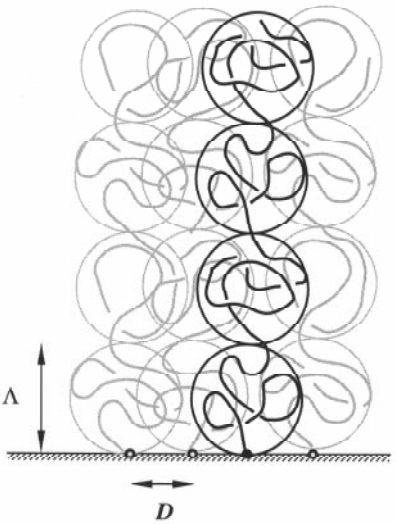

Fig. 8. Schematic of the brush in the region {3b} of the (P,σ) diagram of Fig. 7. Figure adapted from [66]

It is of some interest to build up a scaling picture for the high coverage regime $\sigma > aP^{-1/2}$ (region {5}). As in region {3b}, each chain can be viewed as a string of subunits of size Λ larger than D almost fully stretched along the normal to the wall. At a scale smaller than Λ, the chain behaves like an ideal chain (the corresponding number of monomers is given by $g_\Lambda \cong (L/a)^2$). Within a given subunit, there is on average a number $(\Lambda/D)^2$ of other chains. The subunit size Λ is given by $\Lambda \cong a(D/a)^2$. The kT per subunit ansatz leads to a free energy per chain $F \cong kT\,N/g_\Lambda \cong kT\,N\left(a/D\right)^4$ in agreement with the result found above.

Testing in details the (P,σ) diagram of Fig. 7 is a difficult task. Indeed, in order to check this diagram, one has to use: (a) a technique which gives contrast between the surface and the bulk chains, and (b) a reliable enough way of forming the brushes so that a large range of surface densities can be analyzed. Techniques allowing contrast all imply deuterated polymers, which are not always easy to obtain, and the real control of the surface density and of the brush structure (no adsorption) immediately renders the program difficult: each point in the diagram requires a synthesis and a control of the characteristics of the grafted layer, prior to any further investigation. The general tendency of the diagram of Fig. 7 is the following: increasing the surface density σ or increasing the polymerization index P of the bulk polymer (compared to the polymerization index of the grafted chains, N) lead both to an expulsion of the free chains from the brush, and thus to a decrease of the thickness of the brush profile. Such tendencies are indeed present in the experimental investigations [36, 45, 60, 62], but no systematic experimental test of the theoretical (P,σ) diagram is presently available. In Fig. 9 we present a series of profiles of PDMS brushes obtained by neutrons re-

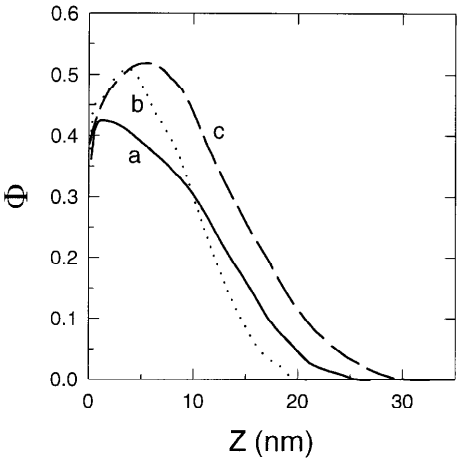

Fig. 9. Concentration profiles determined by neutron reflectivity for three end grafted PDMS layers in contact with PDMS melts. The molecular weight of the grafted chains is mN=92 kg mol^{-1} for all the layers. Curve **a:** surface density in the layer σ= 0.011, molecular weight of the melt mP=90 kg mol^{-1}; curve **b**: σ=0.01, mP=360 kg mol^{-1}; curve **c**: σ= 0.015, mP=17 kg mol^{-1}. The layer contracts more and more when exposed to a melt of larger molecular weight. In all cases the melt chains penetrate down to the surface, as demonstrated by the volume fraction of end grafted chains which always remains much lower than one

flectivity (the grafted chains are deuterated and the bulk polymer is hydrogenated) for several surface densities and different molecular weights of the bulk polymer. Clearly, increasing the surface density and increasing the molecular weight of the bulk polymer, correspond to a progressive expulsion of the bulk chains from the brush, a fact which is apparent first as a reduction of the extension of the concentration profile of the surface chains, and second as an increase in the steepness of this profile. A remarkable feature, however, is that if the tendencies of the experimental profiles do qualitatively agree with the predictions of the diagram of Fig. 7, the real brushes seem to be more easily interpenetrated by bulk chains than predicted. Indeed, even molecular weights much larger than that of the brush do penetrate a brush with a surface density close to $N^{-1/2}$ (Fig. 7). This might be due either to the polydispersity of the grafted chains (even if small, M_w/M_n <1.1), or more generally to the fact that the (P,σ) diagram of Fig. 7 is based on a scaling theory that assumes a step function for the brush segment density profile. For a detailed comparison with the experimental profiles, one has to use analytical self-consistent calculations [52] which relax the constraint of locating all the chain extremities in the same plane [55, 60].

3.2
Irreversibly Adsorbed Layers in Polymeric Matrices

The behavior of an irreversibly adsorbed layer in contact with a melt of shorter, chemically identical chains was studied theoretically by Aubouy et al. [65, 66]. The pseudo-brush was treated as a polydisperse brush of half loops, characterized by the distribution of Eq. (4). Assuming that the local conformation of a polydisperse polymer brush is similar to the bulk structure of a monodisperse brush with the same grafting density, Aubouy and Raphaël [65] built up a diagram analogous to the diagram of Fig. 7. Again, the global tendency is that a dense layer should expel the chains from the melt, and so more efficiently for bulk chains with a large molecular weight. No systematic experimental investigations are presently available, except a few neutrons reflectivity data [36]. Typical examples of profiles are reported in Fig. 10. These results do show an intrinsic difficulty of such investigations: when comparing data for a layer made with either deuterated or hydrogenated PDMS, in contact with a melt of the corresponding either hydrogenated or deuterated chains, a clear preferential interaction of the hydrogenated specie with the silica surface appears. In order to compare the experimentally determined profiles with a model, such a preferential interaction has to be included. On a qualitative level, however, the data seem to indicate that a pseudo-brush is more easily penetrated by a given polymer melt

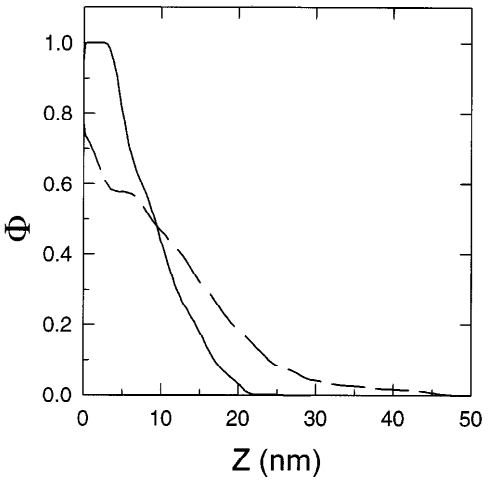

Fig. 10. Concentration profile as determined by neutron reflectivity for two irreversibly adsorbed layers in contact with a PDMS melt. The molecular weight of the surface chains is 92 kg mol^{-1} and is identical to that of the melt. In both cases σ=0.02. The *full line* corresponds to an adsorbed layer made with deuterated chains, in contact with a hydrogenated melt, while the *dotted line* corresponds to the reverse situation (hydrogenated surface chains, deuterated melt). The clear difference between the two profiles is a demonstration of a preferential interaction of the hydrogenated chains with the surface compared to the deuterated one

than the equivalent brush (same surface density and same molecular weight of the surface chains). This might be an indication of the fact mentioned by Laub and Koberstein [67a] that polydispersity may help interdigitation. On the other hand, a pseudo-brush is not really equivalent to a polydisperse brush and one should take the "cactus effect" discussed by Brochard-Wyart et al. [68] into account. The profiles shown inFig. 10 are clearly different from that of a brush: the inner part of the layer is dry (or almost dry in the case of the preferential interactions between the melt and the surface), and tails extend far away from the surface.

4
Role of Surface-Anchored Chains in Adhesion

Understanding what happens when a polymer comes into contact with another material is important for many industrial applications [69, 70]. In the last ten years, there has been a significant improvement in our understanding of the local processes that control the adhesion of polymers [71–73]. Experiments by Hugh Brown and co-workers and by Ed. Kramer and co-workers have shown that the interface between two chemically different glassy polymers can be strengthened by the presence of diblock copolymers at the interface [74–76]. When a fracture propagates at the interface, these coupling chains can either be pulled-out or break. Experiments show that long diblock molecules fail by scission, while shorter diblocks can be pulled out. Random copolymers have also been used recently in this context [77, 78]. Here we shall not discuss adhesion of glassy or semi-crystalline polymers [79–84] but rather focus on the adhesion of elastomers to solids [85–89]. Studies have demonstrated that coupling chains (or "connectors") that bind to the solid and interdigitate with the elastomer enhance the adhesion energy [90]. The important question is to understand how to optimize practical adhesive joints using connector molecules to enhance adhesion. Early models, considering the connector chains as independent of each other, predict a linear increase of the adhesion energy at zero crack propagation velocity, G_0, with the surface density of connectors [91, 92]. So the question is whether it is interesting to graft as many chains as possible on the solid surface. To try to answer this question, systematic experiments on silica/PDMS systems were undertaken, using the pseudo-brushes presented in Sect. 2.1 (these experiments will be discussed in details below). A typical result for G, the adhesive energy measured at a very low velocity of fracture, as a function of the surface density of connector molecules is reported in Fig. 11. The major feature of these data is the non-monotoneous variation of the adhesion energy with σ. The connector molecules clearly loose their efficiency to promote adhesion when they are too densely packed on the surface. Several attempts have been made very recently to try to rationalize such a behavior. They will be reviewed in Sect. 4.1 for the adhesion between a brush and an elastomer and in Sect. 4.2 for the adhesion between a pseudo-brush and an elastomer. Experimental results will be discussed in Sect. 4.3

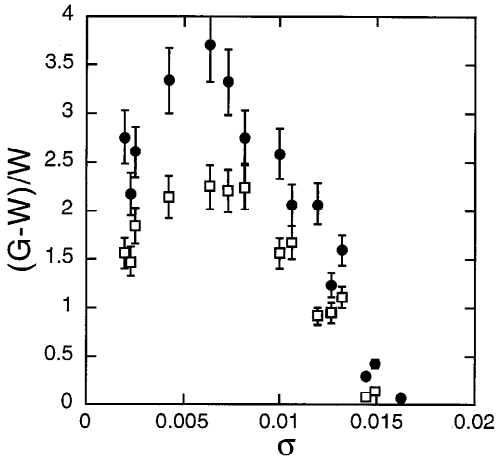

Fig. 11. Normalised enhanced adhesive strength $(G-W)/W$ as a function of the surface density, σ, for two PDMS elastomers in contact with silicon wafers covered with irreversibly adsorbed chains. W is the thermodynamic work of adhesion, $W=2\gamma$, with γ the surface tension of PDMS, $\gamma=21.6$ mN $\cdot$ m^{-1} at 25 °C. The *filled symbols* correspond to a molecular weight between crosslinks in the elastomer $Mc=24.2$ kg mol^{-1} while $M_c=10.2$ kg mol^{-1} for the *open symbols*. The adhesive strength, G, has been measured by peel tests performed at a very low velocity of the propagation of fracture, 0.17 μm/s. The molecular weight of the surface anchored chains is $M_w=242$ kg mol^{-1}

4.1 Adhesion Between a Brush and an Elastomer

The interface between a solid and a crosslinked elastomer can be strengthened by the addition of chains (chemically identical to the elastomer) that are tethered by one end to the solid surface as schematically presented in Fig. 12. As the crack grows along the interface, these coupling chains are progressively pulled-out from the elastomer [71, 90, 93] as schematically presented in Fig. 13. This "suction" process is expected to occur in an approximately plane *cohesive zone* directly ahead of the crack tip [94, 95]. A number of models have been proposed to describe the process of chain pull-out and the relation between chain pull-out and interfacial toughness [91, 92, 96–103]. In the model of Raphaël and de Gennes [92, 100], the partially pulled-out chains are assumed to form single-chain fibrils. The minimization of the sum of the surface and stretching energies of these chains shows that there is a minimum force f^* required for a fibril to exist even at zero pull-out rate (such a minimum force has been observed in a very elegant dewetting experiments by Reiter and co-workers [104]). As the force on a chain that is being pulled-out remains finite as the velocity of the fracture line, V, goes to zero, the existence of a threshold toughness G_0 larger than the thermodynamic work of adhesion W due to intermolecular interactions (typically van

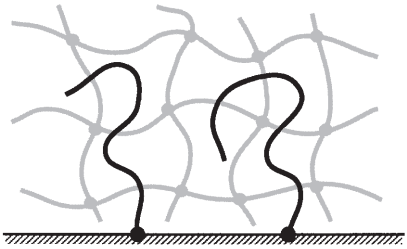

Fig. 12. Schematic representation for an elastomer/solid interface strengthened by the addition of end-grafted chains

der Waals type) is predicted. For many practical cases, the zero-rate fracture energy, G_0, is given by [100, 101]

$$G_0 - W \cong \gamma N \sigma \tag{8}$$

where σ is the dimensionless grafting density of the coupling chains, N their polymerization index, and γ the surface tension of a melt of connector molecules.

Equation (8) is restricted to the limit of low σ, where the connector molecules freely penetrate into the network and have additive contributions. For high σ values, the coupling chains may segregate (at least partially) from the elastomer and G_0 may reduce to W. How to describe the interdigitation between the grafted surface and the network over all the range of σ is a difficult problem which has been recently considered by several authors [3, 68, 105, 106]. Since there are still open questions on the subject, we will here adopt the most simple point of view which is based on the analysis by de Gennes [105] of the equilibrium state between a melt of linear chains (N monomers per chain) and a chemically identical network cross-linked *in the dry state* (N_c monomers between cross-links, with $N_c<N$). Using the fact that the elastic modulus of the network, E, is given by $E \cong kT/a^3 N_c$, de Gennes showed that the behavior of an N-chain inside the net-

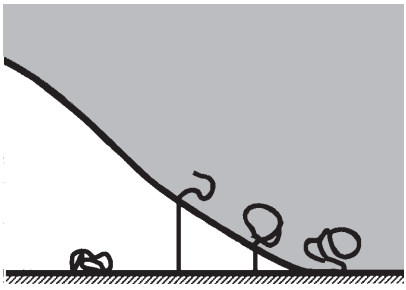

Fig. 13. Schematic picture of the pull-out process that takes place as the crack grows along the interface. As the crack advances, each connector is progressively stretched until it reaches its maximal length. At that point the connectors collapses onto the surface

work is very similar to the behavior of the same N-chain when dissolved in a melt of shorter, chemically identical chains, of length N_c. In the later situation, the short chains screen out the excluded volume interaction, and as shown by Edwards, the effective excluded volume parameter is reduced by a factor $1/N_c$. In the network case, a similar screening occurs through the elastic deformation of the network segments. De Gennes further used the above remarkable analogy to show that the behavior of a polymer brush (N monomers per grafted chain) exposed to a chemically identical network cross-linked in the dry state (N_c monomers between cross-links, with $N_c<N$) is identical to the behavior of the same polymer brush when exposed to a melt of shorter, chemically identical chains, of length N_c. The various regimes of interdigitation between a brush and a network are thus identical to those given in Sect. 3.1 for the interdigitation between a brush and a polymer melt (see Fig. 7).

We can now go back to the evaluation of the adhesion energy between the grafted surface and the elastomer. In all what follows we assume that the elastomer was cross-linked in the dry state. As long as $\sigma<N_c/N^{3/2}$, the local volume fraction of grafted chains, Φ, is much smaller than unity. More precisely, $\Phi<<N_c/N$ for $\sigma<<N_c/N^{3/2}$ (see [105]) and we expect Eq. (8) to hold. For $\sigma>N_c/N^{3/2}$, Eq. (8) should be replaced by [107]

$$G_0 - W \cong \gamma N \sigma \left(1-\Phi\right) \tag{9}$$

where the factor $(1-\Phi)$ is a phenomenological way of taking into account the fact that the connectors interact less and less with the network as Φ increases [67a, 67b]. For $N_c/N^{3/2}<\sigma<N_c^{-1/2}$, Φ is given by $\sigma^{2/3}N_c^{1/3}$ (see Sect. 3.1) and Eq. (9) can be rewritten as

$$G_0 - W \cong \gamma N \sigma \left(1-\sigma^{2/3} N_c^{1/3}\right) \tag{10}$$

For $\sigma>N_c^{-1/2}$, the brush segregates completely from the network and the adhesion energy G_0 reduces to W.

Equation (10) indicates that the adhesion energy passes through an optimum for [3]

$$\sigma_{opt} \approx 0.465 N_c^{-1/2} \tag{11}$$

The corresponding value of G_0 is given by [3]

$$G_{0opt} - W \approx 0.186 \gamma \frac{N}{N_c^{1/2}} \tag{12}$$

The full line in Fig. 14 represents the result of Eq. (10) for N=743 and N_c=230 assuming that $\gamma \approx W/2$ (experimental results with surface chains and elastomers having these characteristics will be presented in Fig. 17).

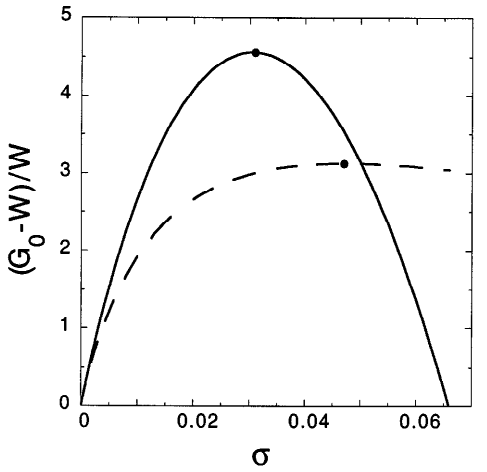

Fig. 14. Normalized enhanced adhesive strength $G_0-W)/W$ vs grafting density σ for a brush (with N=743, N_c=230 and $\gamma \approx W/2$) according to Eq. (10) (*full curve*), and Eqs. (13) and (14) (*dashed curve*). In both cases the optimum is indicated by a *black dot*

Note that if instead of a step-like profile one uses a more realistic profile where Φ is a function of the distance to wall z, Eq. (9) has to be replaced by the more general formula [67a,b,]

$$G_0 - W \cong \gamma \int_a^L \frac{dz}{a} \Phi(z)\left(1-\Phi(z)\right) \tag{13}$$

where L is the brush thickness. In particular, if one uses the SCF results of Zhulina et al. [52] for the case of a brush exposed to a melt (N_c momomers per chain) one obtains

$$G_0 - W \cong \gamma \int_a^{L_{SCF}} \frac{dz}{a} \exp\left[-3\pi^2 N_c \frac{\left({L_{SCF}}^2 - z^2\right)}{8 a^2 N^2}\right] \left(1-\exp\left[-3\pi^2 N_c \frac{\left({L_{SCF}}^2 - z^2\right)}{8 a^2 N^2}\right]\right) \tag{14a}$$

where

$$L_{SCF} = \left(4/\pi^2\right)^{1/3} a N \sigma^{1/3} {N_c}^{-1/3} \tag{14b}$$

One can check numerically that the adhesion energy (Eq. 14a) passes through an optimum. At the level of scaling laws, this optimum has the same characteristics as the optimum predicted by Eq. (10) i.e. $\sigma_{opt} \propto N_c^{-1/2}$ and $G_{0opt} - W \propto \gamma N N_c^{-1/2}$. The dashed line in Fig. 14 presents the result of Eq. (14a) for N=743 and N_c=230 assuming that $\gamma \approx W/2$. The optimum – which is not very visible at the scale of Fig. 14 – is indicated by a black dot.

Let us conclude this section by some remarks [3].

First, the dynamics of interdigitation is expected to be very slow for tethered chains exposed to a network [108]. Thus the above discussion is restricted to long enough times of contact between the brush and the elastomer.

Second, the above discussion is restricted to connectors that are not chemically attached to the elastomer. The opposite situation was analyzed recently by Brochart-Wyart and de Gennes [106] who predicted a switch from adhesive to cohesive rupture.

Third, the above discussion is based on Eq. (8) which is only valid at very low separation velocities. This equation can however be generalized to larger values of V [109].

Finally, the above analysis considers only local crack tip processes. Viscoelastic energy losses during crack propagation [110–113] have been theoretically investigated by de Gennes [114] and by Hui et al. [115], and may also contribute to the sadhesive strength.

4.2 Adhesion Between a Pseudo-Brush and an Elastomer

In order to get an estimate of the adhesion energy between a pseudo-brush and an elastomer (cross-linked in the dry state), we can use the concentration profile calculated [65] for the case of a pseudo-brush exposed to a melt (N_c monomers per chain)

$$\Phi(z) \cong \begin{cases} 1 & a << z << a N_c^{1/2} \phi_0^{7/4} \\ N_c^{1/5} \phi_0^{7/10} (z/a)^{-2/5} & a N_c^{1/2} \phi_0^{7/4} << z << L \end{cases} \tag{15a}$$

with

$$L \cong a N_c^{-1/3} N^{5/6} \phi_0^{7/24} \tag{15b}$$

Inserting Eqs. (15a) and (15b) into Eq. (13), we obtain a quite simple analytical formula for the adhesion energy

$$G_0 - W \cong \gamma N \left\{ \frac{5}{3}\sigma - 5 N_c^{1/3} \sigma^{5/3} + \frac{10}{3} N_c^{1/2} \sigma^2 \right\} \tag{16}$$

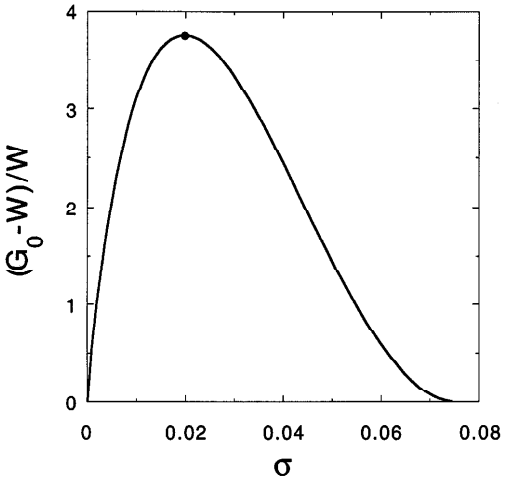

Fig. 15. Normalized enhanced adhesive strength $(G_0-W)/W$ vs grafting density σ for a pseudo-brush (with N=770, N_c=176 and N_c=176) according to Eq. (16) The optimum is indicated by a *black dot*

In Eq. (16), σ is the adimensional surface chain density :$\sigma \approx N^{-1/2}\phi_0{}^{7/8}$.

Equation (16) indicates that G_0 reduces to W for $\sigma \geq N_c{}^{-1/2}$. Equation (16) also indicates that the adhesion energy passes through an optimum for

$$\sigma_{opt} \approx 0.263\, N_c{}^{-1/2} \tag{17}$$

The corresponding value of G_0 is given by

$$G_{0opt} - W \approx 0.129\,\gamma\,\frac{N}{N_c{}^{1/2}} \tag{18}$$

The full line in Fig. 15 represents the result of Eq. (16) for N=770 and N_c=176 assuming that $\gamma \approx W/2$ (to be compared with the experimental data shown in Fig. 17).

Note that Eq. (16) can be rewritten as

$$\frac{G_0 - W}{G_{0opt} - W} = 3.398\left(\frac{\sigma}{\sigma_{opt}}\right) - 4.184\left(\frac{\sigma}{\sigma_{opt}}\right)^{5/3} + 1.787\left(\frac{\sigma}{\sigma_{opt}}\right)^{2} \tag{19}$$

It is interesting to note that at the level of scaling laws, the optimum in the brush/elastomer adhesion energy predicted by Eq. (10) and the optimum in the

pseudo-brush/elastomer adhesion energy predicted by Eq. (16) have the same characteristics [3]:

$$\sigma_{opt} \propto N_c^{-1/2} \tag{20}$$

and

$$G_{0opt} - W \propto \gamma N N_c^{-1/2} \tag{21}$$

These characteristics indicate in particular that one can improve the adhesion between the brush or the pseudo-brush and the elastomer by decreasing the number of monomers between crosslinks, N_c. This result, which is a direct consequence of the de Gennes analogy between a network and a melt (see Sect. 4.1), cannot be correct for too small values of N_c, that is for too highly reticulated networks. For pseudo-brushes, it has been conjectured [107] that Eqs. (20) and (21) are only valid for $N_c > N^{2/3}$ and should be replaced by

$$\sigma_{opt} \propto N_c N^{-1} \tag{22}$$

and

$$G_{0opt} - W \propto \gamma N_c \tag{23}$$

for $N_c < N^{3/2}$.

More theoretical work will be needed to establish the validity of Eqs. (22) and (23), and to derive analogous equations for the brush/elastomer problem.

4.3 Experimental Results

One way to estimate G_0 is to measure the adhesive strengthy G, the energy necessary to open the fracture at finite speed, working at very low speed by using the Johnson-Kendall-Roberts (JKR) technique [116, 117]. In this technique, a lens-shaped elastomer is loaded for a while against a flat solid substrate to allow the adhesion to develop. The load is then removed, and the interfacial crack slowly propagates, driven by the elastic energy stored in the crosslinked elastomer lens [72]. Brown [90] and Creton et al. [93] have used the JKR technique to study chain-pullout process in polyisoprene (PI) where the coupling chains were PS-PI diblock copolymers and the flat substrate was PS (polystyrene). The adhesive strength G was found to increase with diblock copolymer coverage and also with the molecular weight of the PI part of the diblock, in qualitative agreement with Eq. (8).

The adhesion between PDMS chains irreversibly adsorbed on silica and crosslinked PDMS elastomers has been investigated in a systematic way in our group [118–120] over a wider range of surface densities than in the early work by

H.Brown. Both 90° peel test at very low peel velocity (in the range 5 nm/s to 1 μm/s) [118] and JKR test over the same range of fracture velocities were used [121]. The main result of this study is the existence of an optimum surface density to promote the elastomer/solid adhesion, as shown in Fig. 11. The observed loss of efficiency of the connector molecules when increasing their surface density has to be related to the fact that increasing σ leads to a loss of interdigitation (see Sects. 4.1 and 4.2). A remarkable feature of the experimental results is the fact that they display a "universal" behavior: if one plots $(G-W)/(G_{opt}-W)$ as a function of σ/σ_{opt} for elastomers with different molecular weights between crosslinks and for layers made with chains having different molecular weights, all the results gather on a single curve (see Fig. 16), in accordance with the prediction of the simple model of Sect. 4.2 (see Eq. (19) and the corresponding full line in Fig. 16).

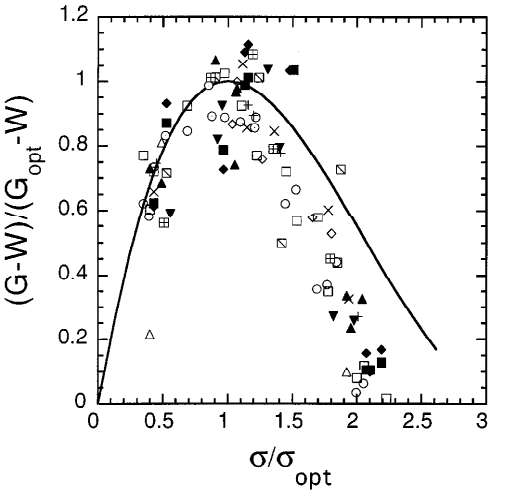

Fig. 16. Universal curve giving the enhanced adhesive strength, G-W, normalized by the optimum enhanced adhesive strength, G_{opt}-W, as a function of the normalized surface density, σ/σ_{opt} (σ_{opt} is the surface density leading to the maximum adhesive strength) for different irreversibly adsorbed PDMS layers in contact with PDMS elastomers. Peel tests with a fracture velocity of 0.017 μm/s have been used to measure G. The molecular weights of the surface chains, M_w, and the molecular weights between crosslinks of the elastomers, M_c, are the following:
(p): M_w=242 kg mol^{-1}, M_c=10.2 kg mol^{-1}; (l): M_w=242 kg mol^{-1}, M_c=24 kg mol^{-1};
(r): M_w=293 kg mol^{-1}, M_c=24 kg mol^{-1}; (×): M_w=293 kg mol^{-1}, M_c=35.4 kg mol^{-1};
(+): M_w=412.5 kg mol^{-1}, M_c=10.2 kg mol^{-1}; (g): M_w=293 kg mol^{-1}, M_c=77.2 kg mol^{-1};
(■): M_w=412.5 kg mol^{-1}, M_c=24 kg mol^{-1}; (R): M_w=412.5 kg mol^{-1}, M_c=35.4 kg mol^{-1};
(▲): M_w=412.5 kg mol^{-1}, M_c=77.2 kg mol^{-1}; (▼): M_w=577.5 kg mol^{-1}, M_c=10.2 kg mol^{-1};
(p): M_w=577.5 kg mol^{-1}, M_c=24 kg mol^{-1}; (⧅): M_w=577.5 kg mol^{-1}, M_c=35.4 kg mol^{-1};
(⊞): M_w=577.5 kg mol^{-1}, M_c=77.2 kg mol^{-1}.
The full line is calculated from Eq. (16)

In order to go further in a detailed comparison between experiments and models, it is convenient to work with end-grafted layers rather than irreversibly adsorbed layers because end-grafted layers are somewhat easier to model. After the first experiments with Creton on chain pull-out effects in the adhesion of polyisoprene [90, 93], Hugh Brown [122] used the same JKR technique to study chain-pullout in PDMS elastomers where the coupling chains where PS-PDMS diblock copolymers and the flat substrate was PS. Surprisingly, Brown essentially observed no effect of the end-grafted chains on the adhesive strength of the interface. We have recently repeated these experiments with PDMS brushes formed by using the method of Folkers et al. [43] described at the end of Sect. 2.1, and have observed pull-out. Typical results are shown in Fig. 17, where the enhancement of adhesive strength of the interface (with a fracture velocity equal to 0.1 μm/s) is reported as a function of σ. For comparison, results for irreversibly adsorbed layers (with similar or much larger molecular weights) in contact with crosslinked PDMS elastomers (with a similar molecular weight between crosslinks) are displayed in the same figure. Both the end-grafted layer and the irreversibly adsorbed layers do give adhesion reinforcement, with an optimum surface density, but this optimum appears sooner (when increasing σ) for the brush than for the pseudo-brush. The pseudo-brush thus appears to be somewhat more efficient to promote adhesion than the equivalent brush. A systematic experimental program is presently underway to establish this result firmly. If confirmed, it will become important to understand what makes the

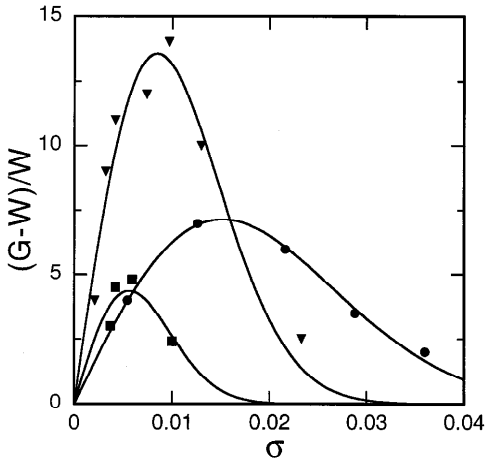

Fig. 17. $(G - W)/W$ as a function of the surface density of connector chains, σ, measured by the JKR test at a velocity of propagation of the fracture of 0.1 μm/s, for 1) (■) a grafted brush with M_w=55 kg mol^{-1} and M_c=17 kg mol^{-1}; 2) (○) an irreversibly adsorbed PDMS layer with M_w=57 kg mol^{-1} and M_c=13 kg mol^{-1}; 3) (▼) an irreversibly adsorbed layer with M_w=140 kg mol^{-1} and M_c=13 kg mol^{-1}. The *full lines* are only guides for the eye, to help to locate the optimum

pseudo-brush more efficient to promote adhesion than the brush[1)]. A natural reason may be the polydispersity of the pseudo-tails. But as mentioned before, a pseudo-brush is not really equivalent to a polydisperse brush and one would have to take into account the "cactus effect" [68].

More theoretical and experimental work is obviously needed for a better understanding of the adhesive properties of surface-anchored polymer chains.

5 Role of Surface-Anchored Chains in Friction

Polymer chains anchored on solid surfaces play a key role on the flow behavior of polymer melts. An important practical example is that of constant speed extrusion processes where various flow instabilities (called "sharkskin", periodic deformation or melt fracture) have been observed to develop above given shear stress thresholds. The origin of these anomalies has long remained poorly understood [123–138]. It is now well admitted that these anomalies are related to the appearance of flow with slip at the wall. It is reasonable to think that the onset of wall slip is related to the strength of the interactions between the solid surface and the melt, and thus should be sensitive to the presence of polymer chains attached to the surface.

Indeed, the shear stress at the solid surface is $\tau_{xz}=\eta_b(\delta V/\delta z)_{z=0}$ (where η_b is the melt viscosity and $(\delta V/\delta z)_{z=0}$ the shear rate at the interface). If there is a finite slip velocity V_s at the interface, the shear stress at the solid surface can also be evaluated as $\tau_{xz}=\beta V_s$, where β is the friction coefficient between the fluid molecules in contact with the surface and the solid surface [139]. Introducing the extrapolation length b of the velocity profile to zero ($b=V_s/(\delta V/\delta z)_{z=0}$, see Fig. 18), one obtains $\beta=\eta_b/b$. Thus, any determination of b will yield β, the friction coefficient between the surface and the fluid. This friction coefficient is a crucial characteristics of the interface: it is obviously directly related to the molecular interactions between the fluid and the solid surface, and it connects these interactions at the molecular level to the rheological properties of the system.

It is important to notice that measuring the shear stress τ_{xz} gives only partial information on the polymer – wall friction, as long as V_s is unknown. Up to 1992, there were no reliable measurements neither of the slip velocity or of the extrapolation length even if direct visualizations of the existence of wall slip had been performed [140]. Migler et al. [141] designed an experimental technique which gives a direct access to the velocity of the fluid very locally at the interface, inside a layer with a typical thickness of 70 nm. This spatial resolution is well adapted to the flows of polymer melts, especially when polymer chains are attached to the wall, the range of the interfacial interactions being of the order of the radius of the polymer chains (between 10 and 100 nm).

We want to review here the main results of these direct measurements of the interfacial velocity, in the case of PDMS melts flowing on silica surface covered

1 The models of Sects. 4.1 and 4.2 are not able to explain this result.

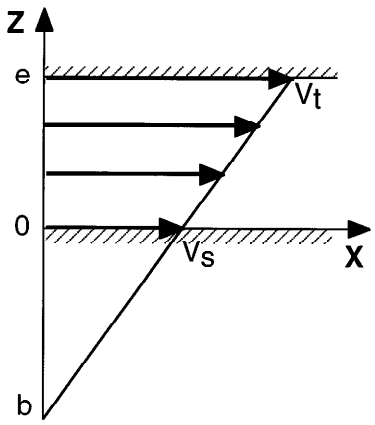

Fig. 18. The simple shear geometry used to characterise the interfacial friction: the fluid thickness is *e*. The top plate limiting the sample is translated at the velocity V_t and transmits this velocity to the fluid. The bottom plate is immobile, and the local velocity of the fluid at the bottom interface is V_s. The fluid is submitted to a simple shear, with a shear rate $\dot{\gamma} = (V_t - V_s)/e$. The velocity profile extrapolates to zero at a distance b below the interface, with the extrapolation length $b = V_s \Big/ \left(\partial V/\partial z\right)_{z=0}$

with various anchored polymer layers, along with the models which have been developed to describe the different friction regimes put into evidence by these experiments.

5.1 The Three Friction Regimes

The polymer system which has been extensively studied was PDMS flowing (simple shear) on smooth silica surfaces bearing either irreversibly adsorbed or end grafted PDMS chains. In the case of adsorbed layers with low densities, it was necessary to protect the surface in order to avoid any further adsorption during the flow experiment (since the surface was put into contact with a PDMS melt). To do so, the silica surface was previously treated by grafting a monolayer of octadecyltrichlorosilane, the adsorption of the surface PDMS chains taking place in the holes of this protective layer which had an adjusted surface density [142]. End grafted layers were produced following the procedure described in Sect. 2.1. Over the range of shear rates explored (from 10^{-2} s^{-1} to 100 s^{-1}), and for all the samples investigated, three different regimes have been observed for the evolution of both the slip velocity and the extrapolation length of the velocity profile as shown in Fig. 19. In Fig. 19a, the average velocity measured in a layer from the interface with a thickness 70 nm, V_s, is displayed as a function of the velocity imposed at the upper limiting surface of the sample, V_t. First, wall slip

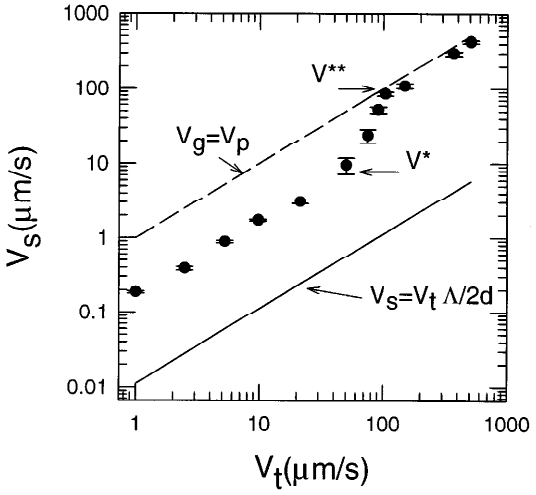

Fig. 19a

exists at all V_t, the measured average local velocity being always at least ten times larger than the average velocity one would obtain in the same layer of fluid, in the case of a zero boundary condition for the velocity at the interface (full line in Fig. 19a). The second clear result is the existence of a transition from low slip to high slip, when the applied shear rate becomes larger than a critical shear rate $\dot{\gamma}^*$. The slip velocity at $\dot{\gamma}^*$ is V^*. In Fig. 19b, the extrapolation length (or slip length) b is reported as a function of the slip velocity V_s. For V_s smaller than V^*, b admits a constant value b_0 (of the order of 1 μm): this is a linear friction regime characterized by a friction coefficient independent of V_s. Between V^* and V^{**}, b becomes proportional to V_s, implying a friction coefficient β inversely propor-

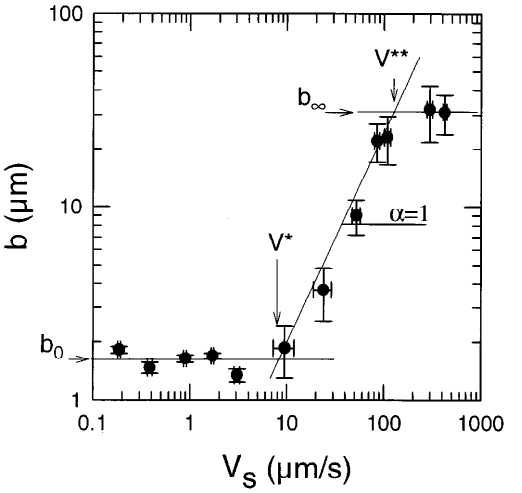

Fig. 19b

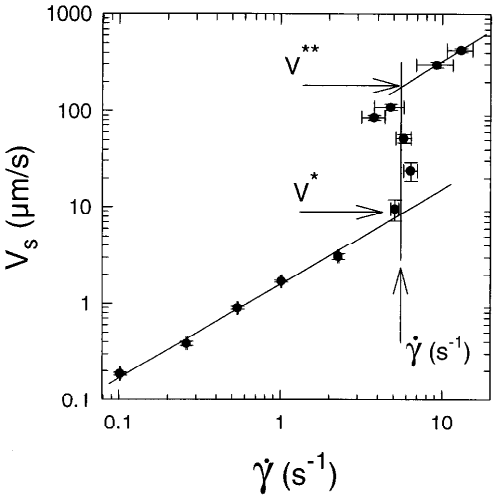

Fig. 19c

Fig. 19a–c. Typical results obtained at the interface between a PDMS melt mP= 970 kg mol-$^{-1}$, with m the molar mass of the monomer m = 0.074 kg/mol) and a grafted PDMS layer (mN=96 kg mol^{-1} and σ=0.0055): **a** the local velocity at the interface V_s (measured in a layer from the interface with a thickness 70 nm) as a function of the imposed top plate velocity V_t; **b** the same data reported in terms of the extrapolation length b as a function of the slip velocity V_s, in log scales. Three different friction regimes are clearly seen: at low shear rates, b is low and constant. Above V^*, b increases linearly with V_s, over more than one decade, and above V^{**}, b becomes constant again with a value b_∞ more than ten times larger than the value at low V_s, b_0; **c** the same data reported in terms of the slip velocity V_s as a function of the shear rate experienced by the polymer melt, $\dot{\gamma}$. The three friction regimes are also clearly visible in this representation. In the marginal regime where b increases linearly with V_s, the shear rate appears locked at the threshold value $\dot{\gamma}^*$

tional to V_s. This non-linear friction regime (the shear stress at the wall is not proportional to the slip velocity) is called the "marginal regime". Finally, for slip velocities larger than V^{**}, b levels off to a value b_∞, about 20 times larger than b_0. In this high slip regime, the friction coefficient between the polymer and the solid is strongly decreased compared to what happens at low velocity, and the polymer melt and the surface are almost decoupled. In Fig. 19c, the variations of the slip velocity vs the shear rate close to the surface, $\dot{\gamma}$ exhibit the same three regimes. The striking feature is that in the whole "marginal regime" $\dot{\gamma}$ remains constant and equal to $\dot{\gamma}^*$.

Such behavior has been interpreted in terms of a molecular model proposed by Brochard-Wyart and de Gennes [143] and further refined [145, 146]. The first version of these models considers a solid surface bearing a few end grafted polymer chains, with a surface density, σ, below the onset of the mushroom regime $\sigma N<1$, with N the polymerization index of the anchored chains). The melt chains have a polymerization index P. Both N and P are assumed to be much larger than N_e, the average number of monomers needed to form an entanglement. Thus the

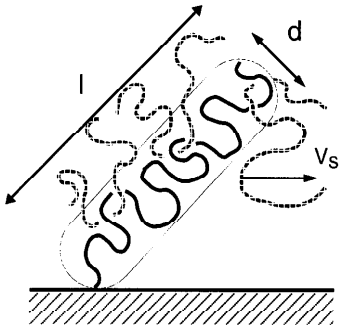

Fig. 20. Schematic representation of one grafted chain entangled with melt chains and deformed under the effect of the friction forces

surface chains behave independently of each other and are entangled with the melt chains which fully penetrate the surface layer. When flowing, the bulk chains exert a friction force on the immobilized surface chains. If large enough, this friction force can deform the surface chains, which in turn develop a restoring elastic force. In a steady state regime these two forces counterbalance. In the first version of the models, the resulting equilibrium shape of the deformed grafted chains was assumed to be a cylinder with a length l and a diameter d, as shown in Fig. 20. In order to evaluate the friction force, let us consider one surface chain and one bulk chain entangled with it. The process allowing the relative motion of these two chains is schematically depicted in Fig. 21: to allow the bulk P chain to flow, the entanglement has to be released in a time shorter than the time taken by the P chain to move parallel to the surface over a distance comparable to the average distance between entanglements, $d^* \cong a N_e^{1/2}$. The velocity of the P chain along its own tube (in the reptation picture [147]) needs thus to be larger than the surface velocity, V_s, by a factor P/N_e. Counting the number of entanglements between the two chains, the friction force f_f between one surface N chain and one bulk P chain can be evaluated as $f_f \cong a \eta_b V_s$. The total friction force between one N chain and the melt is then $F_f \cong X f_f$, where X is the number of bulk chains entangled with one surface chain. F_f increases with V_s, and, consequently, the elongation of the grafted chain increases with V_s. The diameter of the grafted chain is thus a decreasing function of V_s. This description assuming entangled bulk and surface chains, cannot remain valid at large slip velocities: when the diameter of the elongated N chains reaches d^* (that is for $V_s \cong V^*$), one enters into a new friction regime. The cornerstone of the model is that when d reaches d^*, the elongation of the surface chain no longer increases with V_s but remains locked to d^* over a wide range of V_s values. Indeed, if increasing V_s over V^* the diameter of the grafted chain would decrease below d^*, the surface and bulk chains would disentangle, and the friction force would decrease. It would then not be able to balance the large elastic force associated with the large elongation of the N chain which would then recoil and re-entangle. This is the "mar-

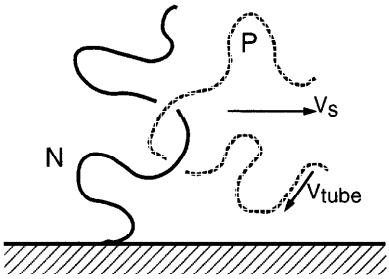

Fig. 21. Schematic representation of the process allowing one melt chain, *P*, entangled with one grafted chain *N* to move parallel to the surface at the velocity V_s: the *P* chain has to release the entanglement fast enough to allow for the relative motion of the two chains. The velocity of the *P* chain along its tube (in the reptation picture) is thus $V_{tube}=V_sP/N_e$ (N_e is the average number of monomers between entanglements)

ginal regime" where the progressive transition from low slip to high slip takes place. It is remarkable that the transition is progressive in terms of the evolution of the extrapolation length with the slip velocity (in Fig. 19, the marginal regime extends over more than one decade in V_s), while it appears sudden in terms of the evolution of the surface stress as a function of the slip velocity: all along the marginal regime, the surface stress is locked at the value τ^*,

$$\tau^* \cong \frac{\sigma kT}{d^* a^2} \cong \eta_b \dot{\gamma}^* \tag{24}$$

while b increases with V_s as

$$b \cong \frac{\eta_b V_s N_e^{1/2} a^3}{\sigma kT} \tag{25}$$

The onset of the marginal regime is reached for $V_s \cong V^*$ with:

$$V^* \cong \frac{kT}{\eta_b N a^2} \tag{26}$$

When the slip velocity is further increased, the Rouse friction [148] finally becomes dominant, for $V_s > V^{**} \propto N^{-1}$. A linear friction regime is then recovered, with a constant extrapolation length, b_∞, much larger than b_0 and comparable to what would be observed on an ideal surface without anchored chains [139].

The experimental data obtained at low surface densities, for end grafted chains, are in very good agreement with these theoretical predictions, not only for the overall evolution of the slip velocity vs the shear rate or of the slip length vs the slip velocity as shown in Fig. 19, but also for the molecular weight dependence of the critical velocity V^* which do follow exactly the laws implied by

Eq. (26): $V^* \propto P^{-3.3} N^{-1}$ [144, 149–152]. The extension of the nonlinear friction regime over a wide range of slip velocities and the reproducibility of the location of the onset of the marginal regime can be taken as clear evidence that the deformation of the surface anchored chains under the effect of the friction force exerted on them by the flowing melt is the correct framework to analyze the dynamic decoupling between the bulk and surface chains. A decoupling mechanism between the melt and the surface based on the breaking or the desorption of the surface chains [153] would lead to a sudden onset of strong slip, the width of the transition being governed by the polydispersity of the surface anchored chains. It would also lead, because the adsorption process is not a rapid one [34], to an evolution of the parameters of the transition (value of the critical shear rate) with the time elapsed under shear, evolution which has never been observed for the PDMS-silica system discussed here.

5.2 Modulation of the Interfacial Friction

From the above discussion, the friction β is given by

$$\beta \cong \frac{\sigma kT}{N_e^{1/2} a V_s} \tag{27}$$

and can be controlled by modulating σ, the surface density of the surface anchored chains. This has been investigated in details by Durliat et al. [151, 152] for end grafted chains. Figure 22 displays the variations of $\dot{\gamma}^*$ vs the grafting density, σ. From $\sigma^*=0.003$ to $\sigma^*=0.01$, $\dot{\gamma}^*$ increases linearly with σ as predicted by Eq. 27. This is surprising, because the model has been developed for surface chains well below the overlapping density, $\sigma^* > N^{-1}$ while the experiments presented in Fig. 22 all correspond to surface densities above the overlapping density: $N \approx 1000$ gives $N^{-1} \approx 0.001$. In fact, σ remains low enough to allow a good penetration of the bulk chains into the surface layer, screening the interactions between the surface chains, so that they still behave independently of each other [6, 65] and the surface stress increases linearly with σ. At the same time, as shown in Fig. 23, the extrapolation length at low slip velocity, b_0, appears to be independent of σ (151). The explanation is due to Gay [144, 145]: the friction between the surface and the melt is fixed by the number of bulk chains entangled with the surface chains. Starting from very low surface densities of grafted chains, and increasing progressively σ, it is natural to think that the number of bulk chains able to entangle with the surface layer first increases linearly with σ. However, the total number of bulk chains trapped by a unit area of the grafted layer cannot increase more than the surface density of bulk chains, $\sigma_b \cong P^{-1/2}$. With X the number of entanglements between one surface chain and one bulk chain, this means that above the grafting density $\sigma_c \cong X^{-1} P^{-1/2}$, the surface layer is saturated with bulk chains and the number of entanglements no longer increases when σ increases. The friction coefficient between the surface chains and the

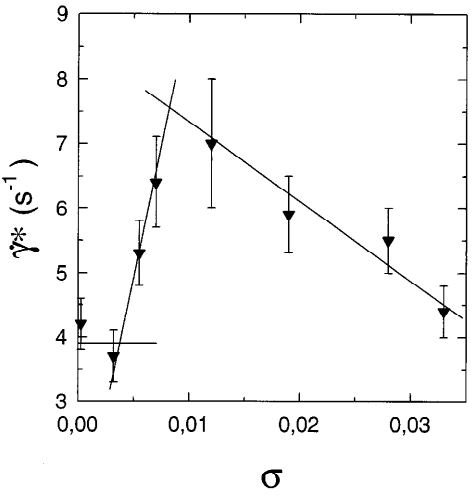

Fig. 22. Evolution of the critical shear rate $\dot{\gamma}^*$ at the onset of the marginal regime as a function of the surface density in the grafted surface layer, σ, for mP=970 kg mol^{-1}, and mN= 96 kg mol^{-1}. For 0.003≤σ≤0.01, $\dot{\gamma}^*$ increases linearly with σ, indicating an additive effect of the surface chains to the friction, i.e. surface chains contributing to the surface friction independently of each other. Above a surface density of 0.01, a collective behavior of the surface chains shows up

fluid is then independent of σ, while the onset of the marginal regime, which corresponds to a given elongation of each surface chain, is characterized by a critical shear rate increasing linearly with σ.

For larger σ values, σ>0.01 in Fig. 22, $\dot{\gamma}^*$ becomes a decreasing function of σ. The friction between the bulk and surface chains is no longer additive as it was at lower surface densities, meaning that a "collective behavior" of the grafted chains shows up. Such a decrease of the critical surface stress for the onset of strong slip means that it becomes easier to disentangle the bulk and surface chains compared to the situation at low surface densities. This is coherent with the fact that the bulk chains are progressively expelled from the surface layer when σ is increased (see Sect. 3.1). Additionally, it is also possible that the mechanical response of the dense grafted layer is different from that at low densities. Up to now there is no quantitative model to describe this situation.

Similar trends have been observed qualitatively for a melt in contact with irreversibly adsorbed layers. Three friction regimes also show up, with a wide marginal regime in which the extrapolation length b follows a power law dependence vs the slip velocity V_s^{α}. Quantitatively, the exponent α of this power law is always smaller than 1 at low grafting density [149] and varies from 0.7 to 1.4 at high grafting densities [151]. At the same time, the shear rate is not exactly locked at a constant value inside the marginal regime, but rather follows a S shape curve as a function of the slip velocity, a fact that can be attributed to the polydispersity of the loops and tails forming the surface anchored layer.

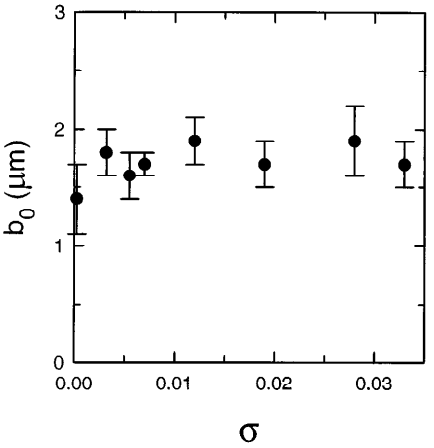

Fig. 23. Evolution of the extrapolation length at low slip velocity, b_0, as a function of the surface density of grafted chains for the experiments reported in Fig. 22. The fact that b_0 appears independent of σ when $\dot{\gamma}^*$ increases linearly with σ indicates that in this range of surface densities, the surface layer has saturated the number of melt chains it can capture

Besides the essential possibility of controlling the surface friction by changing the surface density of anchored chains all other parameters being kept constant, the value of V^* (Eq. 26) can also be adjusted by changing the molecular weight of the anchored chains [150, 152, 154].

The preceding analysis of the progressive decoupling between the surface and bulk chains assumes that the anchored and the bulk chains are entangled, i.e. that N and P are both much larger than N_e. What does happen if this is not the case? An interesting situation should be that corresponding to $N<N_e$, $P>>N_e$ and a high σ value. According to [6, 65] and to the discussion of Sect. 3.1, the bulk chains are then not allowed to penetrate into the dense surface layer of short chains. The surface should thus behave like an ideal one, with a very low friction coefficient, comparable to that observed in the high slip regime previously described. This has indeed been shown by Durliat [151] with small PDMS grafted chains (M_w= kg mol^{-1}, N<N_e) and long PDMS bulk chains (M_w=970 kg mol^{-1}): high slip was always present, even at the lower shear rates experimentally attainable.

All the above results show clearly that adsorbing or grafting polymer chains on a solid surface facing a flowing polymer melt can change drastically the friction coefficient and lead to non trivial non linear friction regimes. For the PDMS/silica system, where the surface chains are strongly anchored to the surface, the dynamic decoupling between the surface and bulk chains occurs through a coil to stretch transition of the surface chains. This leads to a friction governed both by the molecular parameters of the system (surface density of the surface chains, polymerization indices of both the surface and bulk chains) and the level of shear. For weaker anchoring of the surface chains, however, an alter-

native mechanism of decoupling is the desorption of these chains, also leading to an onset of strong wall slip above a critical shear stress and to an abrupt transition [153].

6 Conclusions

There have been considerable advances in understanding adhesion and friction in polymeric systems in the last few years. In this work we have examined in detail the behavior of surface-anchored polydimethylsiloxane chains attached to a plane silica surface. Depending on the fact that either all the monomers in the macromolecule or only one chain extremity are able to bind to the surface, two different categories of layers can be formed (both with controlled molecular characteristics) in a rather wide range of surface density of anchored chains. End-grafted chains form brushes, well described by the SCF parabolic profile of Milner et al. [10, 11] and Zhulina et al. [12] when swollen by a good solvent, while irreversibly adsorbed chains lead to concentration profiles which agree quite well with Guiselin' s description of pseudo-brushes [35].

These surface-anchored layers can be used as adhesion promoters to enhance elastomer-solid adhesive strength. We have shown that there is then an optimum surface density of surface anchored chains to do so. At high coverage of the surface, the layers lose their efficiency, a tendency which can be rationalized in terms of interdigitation between the elastomer and the surface chains. A full characterization of the different regimes of adhesion enhancement associated with the different regimes of interdigitation between the surface chains and the elastomer is a difficult experimental task, not fully accomplished to date.

We have demonstrated that these surface-anchored layers were also quite efficient to adjust the friction between a polymer melt and a surface. This friction is governed by the ability of the surface chains to interdigitate into the melt and to entangle with the bulk chains. However, because the surface anchored chains are flexible and deformable objects, they can elongate under the effect of the friction forces, thus leading to a non-trivial friction law when the local velocity at the interface is progressively increased. Indeed, at sufficiently high shear rates the surface chains become elongated enough so that they can disentangle from the bulk chains, leading to an onset of flow with high slip at the wall, i.e. to a dynamic decoupling between the layer and the bulk polymer. We have shown that it is possible to account for the different observed friction regimes in terms of a molecular model based on this notion of shear induced disentanglement. These investigations thus open the way to the design of surfaces with adjusted friction properties.

An important question is now to understand how these two effects, adhesion enhancement and adjusted friction, can interplay. For example, when peel tests are used to estimate the adhesive strength, the curvature of the peeled ribbon implies a fracture advancing through both modes I and II of opening [72, 155]. This means that in the presence of surface anchored chains, the connector

chains are solicited both in elongation and shear deformation. The total energy necessary to open the fracture, and its velocity dependence should thus be affected by the non-linearity of the interfacial friction. Systematic analysis of such effects just start to appear [156, 157] and should be of great fundamental and practical importance in the near future.

Acknowledgements. We are much indebted to P.-G. de Gennes for stimulating our interest in the behavior of surface-anchored polymer chains; we would like to thank him for his constant and active interest in the work presented here. We have benefited greatly from discussions and collaborations with H. Brown, F. BrochardWyart, M. Tirrell, J. Folkers and K. Migler. We have also benefited from discussions with M. Rubinstein, A. Ajdari, G. Schorsch and L. Vovelle. An important part of the work discussed in the present paper relies on the PhD theses of M. Aubouy, M. Deruelle, E. Durliat, C. Gay, Y. Marciano, C. Marzolin, and G. Massey. We thank them for their essential contribution to this work. We thank C. Creton and M. Aubouy for a critical reading of the manuscript.

7 References

1. Fleer GJ, Cohen Stuart M, Scheutjens J, Cosgrove T, Vincent B (1993) Polymers at interfaces. Chapman & Hall
2. Edwards SF (1994) Faraday Discuss 98:1
3) de Gennes PG (1997) Soft Interfaces (Cambridge University Press).
4. de Gennes PG (1987) Adv Coll Int Sci 27:189
5. Alexander S (1977) J Phys (Paris) 38:977
6. de Gennes PG (1980) Macromolecules 13:1069
7. Hirz SJ (1986) Modeling of interactions between adsorbed block copolymer. M. S. Thesis, University of Minnesota, Minneapolis, MN
8. Cosgrove T, Heath T, van Lent B, Leermakers F, Scheutjens J (1987) Macromolecules 20:1692
9. Skvortsov AM, Pavlushkov IV, Gorbunov AA, Zhulina EB, Borisov OV, Pryamitsin VA (1988) Polymer Sci USSR 30:1706
10. Milner ST, Witten TA, Cates ME (1988) Europhys Lett 5:413
11. Milner ST, Witten TA, Cates ME (1988) Macromolecules 21:2610; Milner ST, Witten TA, Cates ME (1989) Macromolecules 22:853
12. Zhulina EB, Pryamitsyn VA, Borisov OV (1989) Vysokomol Soedin Ser A 31:185
13. Zhulina EB, Borisov OV, Pryamitsyn VA (1990) J Colloid Interface Sci 137:495
14. Murat M, Grest GS (1989) Macromolecules 22:4054
15. Chakrabarti A, Toral R (1990) Macromolecules 23:2016
16. Lai PY, Binder K (1991) J Chem Phys 95:9299
17 Milner ST (1991) Science 251:905
18. Halperin A, Tirrell M, Lodge TP (1991) Adv Polym Sci 100:31
19. Grest GS, Murat M (1995) In: Binder K (ed) Monte Carlo and molecular simulations in polymer science. Oxford University Press, New York, p476
20. Szleifer I, Carignano MA (1996) In: Prigogine I, Rice SA (eds) Advances in chemical physics, vol 94. Wiley, New York, p165
21. Vincent B (1974) Adv Colloid Interface Sci 4:193
22) Napper D (1983) Polymeric stabilisation of colloidal dispersions. Academic Press
23. Klein J (1989) Physics World, 2 June
24. Taunton HJ, Toprakcioglu C, Fetters LJ, Klein J (1988) Nature 332:712
25. Auroy P, Auvray L, Léger L (1991) Macromolecules 24:2523
26. Auroy P, Auvray L, Léger L (1991) Macromolecules 24:5158

27. Auroy P, Auvray L, Léger L (1991) Phys Rev Letters 66:719
28. Hadziioannou G, Patel S, Granick S, Tirrell M (1986) J Amer Chem Soc 108:2869
29. Tirrell M, Patel S, Hadziioannou G (1987) Proc Nat Acad Sci 84:4725
30. Granick S, Herz J (1985) Macromolecules 18:460
31. Factor BJ, Lee LT, Kent MS, Rondelez F (1993) Phys Rev E 48:2354
32. Kent MS, Lee LT, Factor BJ, Rondelez F, Smith GS (1995) J Chem Phys 103:2320
33. Bates FS (1991) Science 251:898
34. Cohen Addad JP, Viallat AM, Pouchelon A (1986) Polymer 27:843
35. Guiselin O (1992) Europhys Lett 17:225
36. Marzolin C (1995) PhD Thesis, University Paris VI, France
37. Deruelle M, Ober R, Vovelle L, Hervet H, Léger L (to be published)
38) Deruelle M, PhD Thesis (1995) University Paris VI, France
39. de Gennes PG (1981) Macromolecules 14:1637
40. de Gennes PG (1982) Macromolecules 15:492
41. Auvray L, Cotton JP (1987) Macromolecules 20:202
42. de Gennes PG (1985) Scaling concepts in polymer physics. Cornell Univ Press, Ithaca
43. Folkers JP, Deruelle M, Durliat E, Marzolin C, Hervet H, Léger L (submitted to Macromolecules)
44. Pincus P (1991) Macromolecules 24:2912
45. Marzolin C, Menelle A, Hervet H, Léger L (submitted to Macromolecules)
46. Leibler L (1988) Makromol Chem, Macromol Symp 16:1
47. Shull KR (1991) J Chem Phys 94:5723
48. Zhulina EB, Borisov OV (1990) J Colloid Interface Sci 144:507
49. Zhulina EB, Borisov OV, Brombacher L (1991) Macromolecules 24:4679
50. Wijmans CM, Scheutjens JMHM, Zhulina EB (1992) Macromolecules 25:2657
51. Raphaël E, Pincus P, Fredrickson GH (1993) Macromolecules 26:1996
52. Wijmans CM, Zhulina EB, Fleer GJ (1994) Macromolecules 27:3238
53. Aubouy M, Raphaël E (1993) J Phys II France 3:443
54. Aubouy M, Fredrickson GH, Pincus P, Raphaël E (1995) Macromolecules 28:2979
55. Wijmans CM, Factor BJ (1996) Macromolecules 29:4406
56. Shull KR (1996) Macromolecules 29:2659
57. Budkowski A, Steiner U, Klein J, Fetters LJ (1992) Europhys Lett 20:499
58. Budkowski A, Klein J, Steiner U, Fetters LJ (1993) Macromolecules 26:2470
59. Jones RAL, Norton LJ, Shull KR, Kramer EJ, Felcher GP, Karim A, Fetters LJ (1992) Macromolecules 25:2359
60. Clark CJ, Jones RAL, Kramer EJ, Shull KR, Penfold J (1995) Macromolecules 28:2042
61. Auroy P, Auvray L (1996) Macromolecules 29:337
62. Lee LT, Factor BJ, Rondelez F, Kent M (1994) Faraday Discuss 98:139
63. Zhao X, Zhao W, Zheng X, Rafailovich MH, Sokolov J, Schwarz SA, Pudensi MAA, Russell TP, Kumar SK, Fetters LJ (1992) Phys Rev Lett 69:776
64. Grest GS (1996) J Chem Phys 105:5532
65. Aubouy M, Raphaël E (1994) Macromolecules 27:5182
66. Aubouy M (1995) Ph.D Thesis, Pierre and Marie Curie University, Paris; Aubouy M, Guiselin O, Raphaël E (1996) Macromolecules 29:7261
67. (a) Laub CF, Koberstein JT (1994) Macromolecules 27:5016; (b) Creton C, Kramer EJ, Hui CY, Brown HR (1992) Macromolecules 25:3075
68. BrochardWyart F, de Gennes PG, Léger L, Marciano Y, Raphaël E (1994) J Chem Phys 98:9405
69. Wool RP (1995) Structure and strength of polymer interfaces. Hanser/Gardner Publications, NY
70. Brown HR (1996) Physics World, January:38
71. Brown HR (1991) Ann Rev Mat Sci 21:463
72. Brown HR (1994) IBM J Res Develop 38:379
73. Baljon ARC, Robbins MO (1996) Science 271:483

74. Brown HR, Deline VR, Green PF (1989) Nature 341:221
75. Creton C, Kramer EJ, Hadziioanou (1991) Macromolecules 24:1846
76. Creton C, Kramer EJ, Hui CY, Brown HR (1992) Macromolecules 25:3075
77. Brown HR, Char K, Deline VR, Grenn PF (1993) Macromolecules 26:4155
78. Dai CA, Dair BJ, Dai KH, Ober CK, Kramer EJ, Hui CY, Jelinski LW (1994) Phys Rev Lett 73:2472
79. Duchet J, Chapel JP, Chabert B, Spitz R, Gerard JF (1997) J Appl Polym Sci 65:2480
80. Gérard JF, Chabert B (1996) Macromol Symp 108:137
81. Lin R, Wang H, Kalika DS, Penn LS (1996) J Adhesion Sci Tech 10:327
82. Lin R, Quirk RP, Kuang J, Penn LS (1996) J Adhesion Sci Tech 10:431
83. Boucher E, Folkers JP, Hervet H, Léger L, Creton C (1996) Macromolecules 29:774
84. Boucher E, Folkers JP, Creton C, Hervet H, Léger L (1997) Macromolecules 30:2102
85. Shanahan MER, Schreck P, Schultz J (1988) C R Acad Sci (Paris) II 306:1325
86. Vallat MF, Ziegler P, Pasquet V, Schultz J (1990) C R Acad Sci (Paris) II 310:477
87. Shanahan MER, Michel F (1991) Int J Adhes Adhes 11:170
88. Maugis D (1991) J Colloid Interface Science 150:243
89. Nardin M, Alloun A, Schultz J (1993) Proceedings of the 16th Annual Meeting of the Adhesion Society, Williamsburg
90. Brown HR (1993) Macromolecules 23:1666
91. de Gennes PG (1989) J Phys France 50:2551
92. Raphaël E, de Gennes PG (1992) J Phys Chem 96:4002
93. Creton C, Brown HR, Shull KR (1994) Macromolecules 27:3174
94. de Gennes PG (1990) Canadian J of Phys 68:1049
95. Fager LO, Bassani JL, Hui CY, Xu DB (1991) Int J Fracture Mech 52:119
96. de Gennes PG (1989) C R Acad Sci (Paris) II 309:1125
97. Xu DB, Hui CY, Kramer EJ, Creton C (1991) Mech Mater 11:257. This model is aimed mainly at the pullout process in glassy polymers
98. Hong JI, de Gennes PG (1993) Macromolecules 26:520
99. Rubinstein M, Ajdari A, Leibler L, BrochardWyart F, de Gennes PG (1993) C R Acad Sci (Paris) II 316:317
100. Raphaël E, de Gennes PG (1994) In: Bruisma R, Rabin Y (eds) Soft order in physical systems. Plenum Press, NY
101. Brown HR, Hui CY, Raphaël E (1994) Macromolecules 27:607
102. Ligoure C (1996) Macromolecules 29:5459
103. Ligoure C, Harden JL (1997) J Phys Chem B 101:4613
104. Reiter G, Schultz J, Auroy P, Auvray (1996) Europhys Lett 33:1
105. de Gennes PG (1994) C R Acad Sci (Paris) II 318:165
106. BrochardWyart F, de Gennes PG (1996) J of Adhesion 57:21
107. Léger L, Raphaël E (1995) In: Daillant J, Guenoun P, Marques C, Muller P, Tran Than Van J (eds) Short and long chains at interfaces. Editions Frontières, GifsurYvette
108. O'Connor KP, McLeish TCB (1993) Macromolecules 26:7322
109. Marciano Y, Raphaël E (1994) Int Journ of Fracture 67:R23
110. Gent AN, Petrich R (1969) Proc R Soc London A 310:433
111. Gent AN, Schultz J (1972) J Adhes 3:281
112. Andrews EH, Kinloch AJ (1973) Proc R Soc London 332:385
113. Carré A, Schultz J (1984) J Adhes 18:171
114. de Gennes PG (1988) C R Acad Sci (Paris) II 307:1949
115. Hui CY, Xu DB, Kramer EJ (1992) J Appl Phys 72:3294
116. Johnson KL, Kendall K, Roberts AD (1971) Proc R Soc London A 324:301
117. Chaudhury MK, Whitesides GM (1991) Langmuir 7:1013
118. Marciano Y (1994) PhD Thesis, University Paris XI France
119. Deruelle M, Tirrell M, Marciano Y, Hervet H, Léger L (1994) Faraday Discuss 98:55
120. Deruelle M, Léger L, Tirrell M (1995) Macromolecules 28:7419
121. Deruelle M, Hervet H, Jandeau G, Léger L (1998) Adhesion Sci. Technol. 12:225

122. Brown HR (1995) (unpublished results)
123. ShiQuing W, Drda PA (1996) Macromolecules 29:2627
124. Benbow JJ, Lamb P (1963) SPE Trans 3:7
125. de Smet, Nam S (1987) Plastic Rubber Process Appl 8:11
126. Denn MM (1990) Ann Rev Fluid Mech 22:13
127. El Kissi N, Léger L, Piau JM (1994) J Non Newtonian Fluid Mech 52:249
128. El Kissi N, Piau JM (1990) J Non Newtonian Fluid Mech 37:55
129. Hatzikiriakos SG, Dealy JM (1991) J Rheol 35:497
130. Hatzikiriakos SG, Dealy JM (1992) J Rheol 36:703
131. Hatzikiriakos SG, Dealy JM (1992) J Rheol 36:845
132. Kalika DS, Denn MM (1987) J Rheol 31:815
133. Larson RG (1992) Rheol. Acta 31:213
134. Piau JM, El Kissi N (1994) J Non Newtonian Fluid Mech 54:121
135. Piau JM, El Kissi N (1994) J Rheol 38:1447
136. Piau JM, El Kissi N, Tremblay BJ (1990) J Non Newtonian Fluid Mech 34:145
137. Ramamurthy AV (1986) J Rheol 30:337
138. Vinogradov GV, Protasov VP, Dreval VE (1984) Rheol Acta 23:46
139. de Gennes PG (1979) CR Acad Paris 288:219
140. Atwood BT, Schowalter WR (1989) Rheol Acta 28:134
141. Migler KB, Hervet H, Léger L. (1993) Phys Rev Lett 70:287
142. Silberzan P, Léger L, Ausserré D, Benattar JJ (1991) Langmuir 7:1647
143. BrochardWyart F, de Gennes PG (1992) Langmuir 8:3033
144. Leger L, Hervet H, Marciano Y, Deruelle M, Massey G (1995) Israel J Chem 35:65
145. BrochardWyart F, Gay C, de Gennes PG (1996) Macromolecules 29:1992
146. Gay C (1997) PhD Thesis, University Paris VI (France)
147. (a) de Gennes PG (1971) J Chem Phys 55:572; (b) Ajdari A, BrochardWyart F, Gay C, de Gennes PG, Viovy JL (1995) J. Phys. II France 5:491
148. Rouse PE (1953) J Chem Phys 21:1273
149. Massey G (1996) PhD Thesis, University Paris VI (France)
150. Léger L, Hervet H, Massey G (1996) In: Piau JM, Agassant JF (eds) Rheology for polymer melt processing. Elsevier, p 337
151. Durliat E (1997) PhD Thesis, University Paris VI (France)
152. Durliat E, Hervet H, Leger L (1997) Europhys Lett 38:383
153. Yongwoo I, ShiQuing W (1996) Phys Rev Lett 76:467
154. Massey G, Hervet H, Léger L (1998) Europhys Lett 43:83
155. Kanninen M, Popelar C (1985) Advanced Fracture Mechanics. Oxford University Press
156. Brown H (1994) Science 263:1411
157. Newby BZ, Chaudhury MK (1997) Langmuir 13:1805

Received: February 1998